International Scholarly Research Network
ISRN Condensed Matter Physics
Volume 2012, Article ID 732973, 21 pages
doi:10.5402/2012/732973

Review Article

Electrodynamics of Bechgaard Salts: Optical Properties of One-Dimensional Metals

Martin Dressel

1. Physikaliisches Insitut, Universität Stuttgart, Pfaffenwaldring 57, 70550 Stuttgart, Germany

Correspondence should be addressed to Martin Dressel, http://www.pi1.uni-stuttgart.de/

Received 21 June 2012; Accepted 10 July 2012

Academic Editors: H. Eisaki, I. Galanakis, H. D. Hochheimer, C. Homes, Y. Ohta, and J. Tempere

The electrodynamic properties of the quasi-one-dimensional organic conductors $(TMTSF)_2X$ are discussed, with particular emphasis on important deviations from the simple Drude model, the transition from a Luttinger-liquid to a Fermi-liquid behavior at the dimensional crossover when pressure is applied or temperature reduced, indications of a pseudogap as well as a low-frequency collective mode. Superconductivity and spin-density-wave ground states breaking the symmetry and gaps should occur in the excitation spectra. The previous literature is summarized and the current status of our understanding presented. Novel THz experiments on $(TMTSF)_2PF_6$ and $(TMTSF)_2ClO_4$ not only shine light into some of the open questions, but also pose new ones.

1. Introduction

Physics in one dimension is a fascinating topic for theory and challenging for experiments. One-dimensional models are simpler compared to three-dimensional ones; in many cases, analytical solutions exist only in one dimension, while numerical approaches have to be used in higher dimensions [1]. Often the reduction of dimensionality does not really matter because the essential physics remains unaffected. But there are also a number of phenomena in condensed matter which only or mostly occur in one dimension. In general, the dominance of the lattice is reduced and electronic interactions become superior. This implies that physics in reduced dimensions is physics of low energies; the relevant effects do not occur in the electron-volt range but at millielectron volts and below. Quantum mechanical effects are essential as soon as the confinement approaches the electron wavelength. Fundamental concepts of physics, like the Fermi liquid theory of interacting particles breaks down in one dimension and has to be replaced by alternative concepts based on collective excitations [2].

One-dimensional structures are intrinsically unstable for thermodynamic reasons. Hence various kinds of ordering phenomena may take place which break the translational symmetry of the lattice, charge, or spin degrees of freedom: phase transitions occur as a function of temperature or some order parameter. On the other hand, fluctuations suppress long-range order at any finite temperature in one (and two) dimension. The ordered ground state is only stabilized by the fact that real systems consist of one-dimensional chains, which are coupled to some degree. The challenge now is to extract the one-dimensional physics from experimental investigations of quasi-one-dimensional systems and to check the theoretical predictions. Besides pure scientific interest, the crucial importance of these phenomena in nanotechnology might not lie ahead too far.

After a short overview of some milestones in the development of quasi-one-dimensional crystalline structures, the electrodynamic properties of the Bechgaard salts are discussed in detail, as they serve as the superior model systems of quasi-one-dimensional conductors. More than 30 years after the first optical spectra on the quasi-one-dimensional organic superconductor $(TMTSF)_2PF_6$ were published by Jacobsen et al. [3], the electrodynamic properties of the Bechgaard salts are still puzzling and subject to continuous experimental and theoretical efforts. Several issues make the materials and their physical properties so interesting and challenging.

(i) The metallic properties are extremely anisotropic; this makes these organic salts the prime examples to study one-dimensional physics.

(ii) The optical reflectivity and conductivity deviate from the simple Drude model; while there is a plasma edge present like in regular metals, the low-frequency properties exhibit very unusual behavior, not all of them are well understood by now.

(iii) The conduction electrons cannot be described by the Fermi liquid theory but exhibit the scaling behavior of a Tomonaga-Luttinger liquid.

(iv) A pseudogap seems to open in the far-infrared frequency range at low temperatures; this reduced spectral weight might correspond to the extremely low density of electronic states observed by photoemission spectroscopy.

(v) The broken-symmetry ground states—such as charge density wave, spin density wave, or superconducting states—exhibit their particular fingerprint in the electrodynamic properties, single-particle gaps as well as collective excitations.

(vi) But even in the metallic state, there are indications of collective modes observed in the THz range of frequency.

1.1. One-Dimensional Metal: Pt-Chains. The low-frequency electrodynamic properties of one-dimensional metals in general and organic conductors in particular have puzzled researches for decades. Although theoretically discussed for a long time [7], it all started in the early 70s of the last century with the Krogmann salt $K_2Pt(CN)_4Br_{0.3} \cdot H_2O$, known as KCP, that consists of a chain of platinum ions with overlapping d orbitals [8, 9]. In Figure 1, the optical reflectivity and conductivity of KCP are displayed for different temperatures and polarizations [4, 5]. The room temperature conductivity of KCP along the chain direction is very high $\sigma_{\|} = 10^2\,(\Omega\,\mathrm{cm})^{-1}$; the anisotropy ratio is $\sigma_{\|}/\sigma_{\perp} = 10^5$. Due to the anisotropic nature, the reflectivity $R(\omega)$ shows a plasma edge only for the electric field $\mathbf{E}$ along the chains ($E\|z$) while it remains low and basically frequency independent perpendicular to it, as known from dielectrics and other insulators. At low temperatures, the single-particle gap around $1000\,\mathrm{cm}^{-1}$ becomes more pronounced, and an additional structure is observed in the far-infrared conductivity which is assigned to the pinned-mode resonance induced by the charge density wave (Figure 1(b)). A detailed investigation of the pinned-mode resonance, its center frequency and lineshape, and furthermore its dependence on temperature and impurity content turned out to be extremely difficult because it commonly occurs in the range of 3 to 300 GHz (0.1 to $10\,\mathrm{cm}^{-1}$); that is, it falls right into the gap between high-frequency experiments using contacts and optical measurements by freely travelling waves [10]. Microwave technique based on resonant cavities and quasi-optical THz spectroscopy was advanced over the years in order to bridge this so-called THz gap [11–16].

1.2. First One-Dimensional Organic Conductor: TTF-TCNQ. The breakthrough in the field of one-dimensional organic conductors happened around the same time with the synthesis of tetrathiafulvalene-tetracyanoquinodimethane (TTF-TCNQ), which exhibits a room temperature conductivity of $10^3(\Omega\mathrm{cm})^{-1}$ and an anisotropy of more than a factor of 100 [7, 17–19]. In Figure 2, the optical properties of TTF-TCNQ are presented [6]. Clear deviations from the Drude behavior of a conventional metal [10] are observed due to the one-dimensional nature. The most surprising fact is the somewhat low reflectivity and conductivity in the far-infrared range. This discrepancy between the high dc conductivity and the low far-infrared conductivity seems to be a generic feature found in all one-dimensional conductors. Although the dc conductivity increases by more than an order of magnitude by cooling from room temperatures down to $T = 60\,\mathrm{K}$ [20–22], the infrared conductivity remains low (Figure 2(b)). When the temperature is reduced below the $T_{\mathrm{CDW}} \approx 53\,\mathrm{K}$, the low-frequency reflectivity drops because an energy gap opens at the Fermi level.

In their first infrared transmission and reflection studies on TTF-TCNQ films and single crystals, Tanner et al. observed that within the energy gap of $1050\,\mathrm{cm}^{-1}$ a collective mode develops in the optical conductivity at zero energy that moves to finite frequencies as $T < T_{\mathrm{CDW}} = 53\,\mathrm{K}$ [20, 21, 23–30]. They conclude that a collective charge-density-wave mode develops below T_{CDW} that is centered around $80\,\mathrm{cm}^{-1}$ due to pinning by impurities and contains an oscillator strength of $500\,\mathrm{cm}^{-1}$; this corresponds to an effective mass of $m^* = 300m_b$ with a bandmass $m_b = 3m_0$ [10]. The issue is not settled yet, but the interpretation seems questionable since the center frequency is too high, implying unreasonably strong coupling. The situation in TTF-TCNQ contains the particular complication of two stacks (TTF and TCNQ), both developing a charge density wave with some interaction. An alternative interpretation of the $80\,\mathrm{cm}^{-1}$ peak would be optical excitations across the Mott gap.

It is quite interesting that the extremely high dc conductivity in the metallic regime above the charge-density-wave transition could barely be reconciled with the optical properties. Some spectral weight is shifted toward low frequencies upon cooling, which infers improved metallic conductivity. Nevertheless, there is a positive slope in $\sigma_1(\omega)$ at any temperature, indicating a pseudogap and effectively reducing the far-infrared conductivity. It was suggested that the Drude-like mode with a plasma frequency of approximately $10^4\,\mathrm{cm}^{-1}$ exhibits a width of only $1/(2\pi\tau c) = 0.5\,\mathrm{cm}^{-1}$ as depicted in Figure 3. This is confirmed by the dielectric constant (or the imaginary part of the conductivity $\sigma_2(\omega)$) that evidences considerable spectral weight at very low frequencies, that is, below $10\,\mathrm{cm}^{-1}$. It should be noted here that the data are taken at a temperature $T = 60$–$85\,\mathrm{K}$, where such a narrow response can only be imagined if phonons scattering does not contribute considerable to the broadening, a fact rather common to one-dimensional metals.

1.3. Fabre and Bechgaard Salts $(TMTTF)_2X$ and $(TMTSF)_2X$. In late 1970s, Fabre and Bechgaard succeeded to suppress the charge-density-wave metal-insulator transition

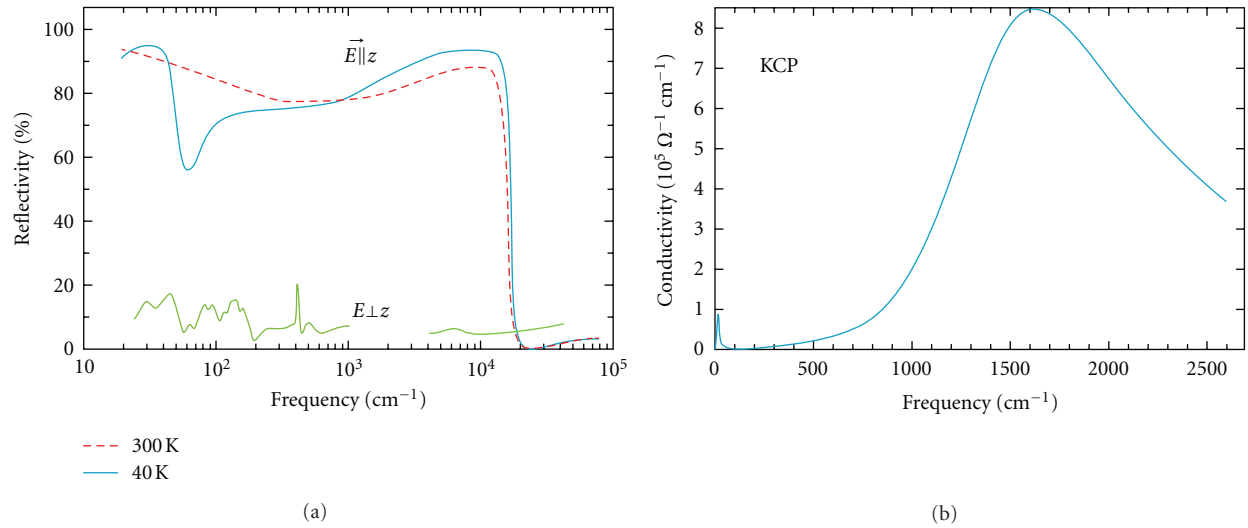

FIGURE 1: (a) Reflectivity of $K_2Pt(CN)_4Br_{0.3} \cdot H_2O$ (abbreviated KCP) measured parallel and perpendicular to the chains at different temperatures as indicated. (b) Optical conductivity of KCP for $\mathbf{E}\|$ stacks at $T = 40$ K (after [4, 5]). The excitations across the single-particle Peierls gap lead to a broadband in the mid-infrared while the small and sharp peak centered around 15 cm^{-1} is due to the pinned mode.

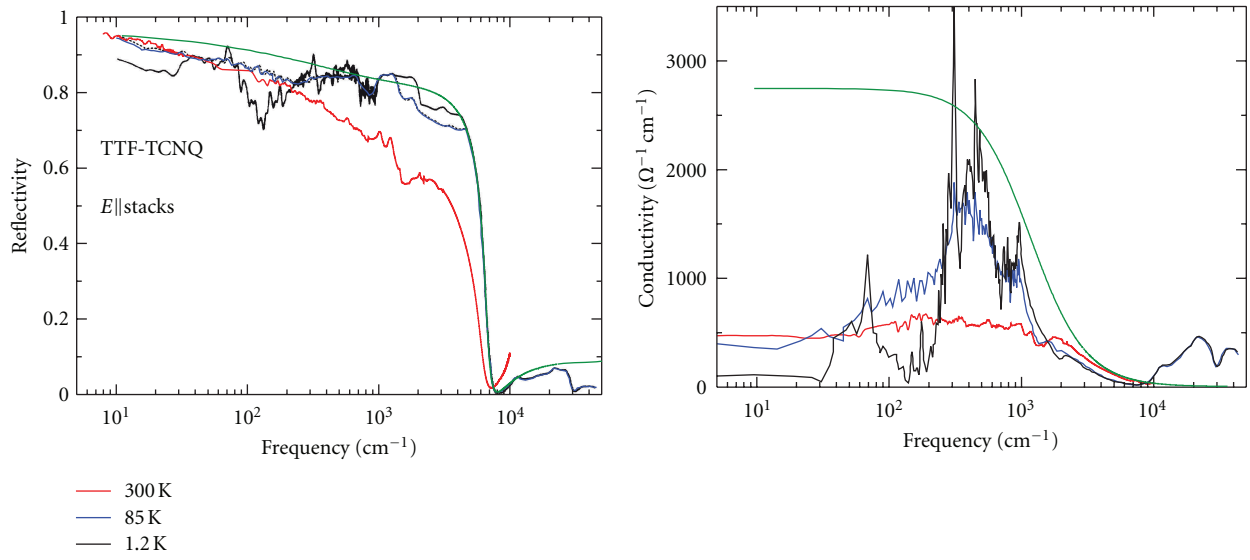

FIGURE 2: (a) Optical reflectivity and (b) conductivity of TTF-TCNQ parallel to the stack direction b for temperatures above and below the charge-density-wave transition $T_{CDW} = 53$ K (some data taken from Basista et al. [6]). The insulating state is seen by the drop in the low-frequency reflectivity. The suppression of the conductivity below 300 cm^{-1} indicates the opening of the charge-density-wave gap. For comparison, the thin green lines represent the simple metallic behavior according to the Drude model with a plasma frequency of $\omega_p/(2\pi c) = 42000$ cm^{-1} and a scattering rate of $1/(2\pi\tau c) = 1200$ cm^{-1}.

by enlarging the organic molecule from TTF to TMTTF and TMTSF, which stands for tetramethyltetrathiofulvalene and tetramethyltetraselenafulvalene, respectively [19, 31–35]. Single crystals are usually grown by electrochemical methods and reach a size of several millimeters in length and less than a millimeter in width. All compounds of the TMTTF and TMTSF family are isostructural. Due to the triclinic symmetry, b' denotes the projection of the b axis perpendicular to a, and c^* is normal to the ab plane.

Because of the stronger coupling between the stacks, the TMTSF salts are electronically more two dimensional, as seen by the appreciable warping of the Fermi surface. Metallic behavior is reached down to lower temperatures (Figure 4), and $(TMTSF)_2ClO_4$ even enters the superconducting state

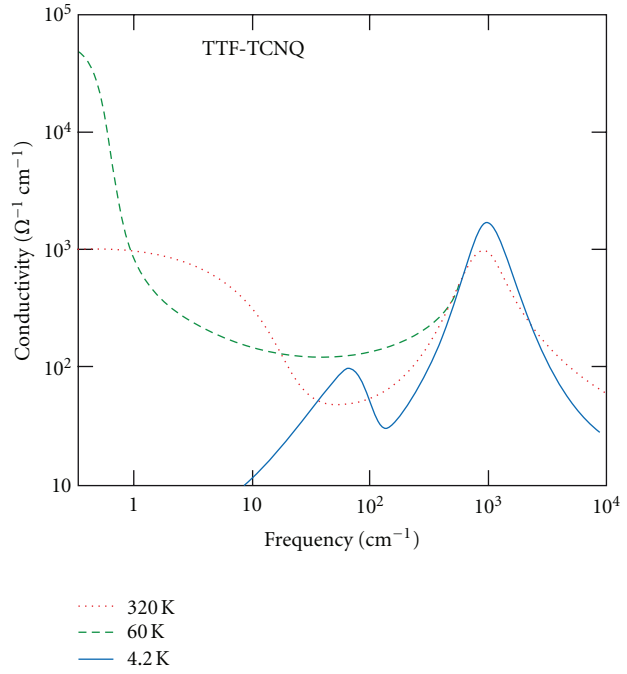

Figure 3: Schematic picture of the real part of the optical conductivity of TTF-TCNQ along the chain direction, at three temperatures, after Tanner et al. [25]. The experiments include microwave, far- to near-infrared and cover a wide range from 0.3 to 10^4 cm^{-1}.

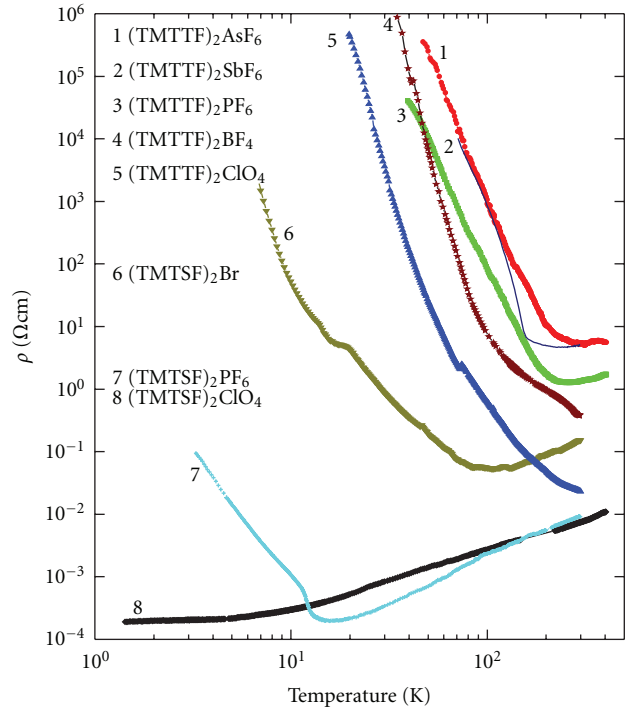

Figure 4: Temperature dependence of the dc resistivity of several Fabre and Bechgaard salts. As the temperature is reduced, the charges become increasingly localized in (TMTTF)$_2$AsF$_6$ and (TMTTF)$_2$PF$_6$, before the charge-ordered state is entered below 100 K. (TMTTF)$_2$SbF$_6$ shows a transition from a metal-like state directly into the charge-ordered state at $T_{CO} = 157$ K. (TMTSF)$_2$PF$_6$ undergoes a SDW transition at $T_{SDW} = 12$ K. Only (TMTSF)$_2$ClO$_4$ remains metallic all the way down to approximately $T_c = 1.2$ K where it becomes superconducting (after Dressel et al. [36–39]).

at $T_c \approx 1$ K when cooled slowly, as presented later in Figure 7(b). (TMTSF)$_2$PF$_6$ undergoes a spin-density-wave transition at 12 K, which can be suppressed by hydrostatic pressure [50]. Since 30 years both compounds serve as prime examples of one-dimensional metals, and enormous effort was put in exploring the low-energy electrodynamics in the search for the pseudogap, the Drude-like component, the collective mode, Luttinger- or Fermi-liquid behavior, dimensional crossover, and so forth. In Figure 5, the various results are compiled by plotting the absorption $A(\omega) = 1 - R(\omega)$ as a function of frequency on a double logarithmic scale, in order to highlight the low-frequency and high-reflectivity part.

Even after a quarter of a century, the extended reviews by Jacobsen [51–53] still give the best overview on the optical properties of Bechgaard salts, the theoretical background, and thorough discussion of their implication.

2. Dimensional Crossover

In their seminal paper, Jacobsen et al. [3] already realized that (TMTSF)$_2$PF$_6$ exhibits a plasma edge in the optical reflectivity not only along the stacking direction a, that becomes more pronounced as the temperatures decreases below $T = 300$ K. At low temperatures a plasma edge is also seen for $E \| b'$, although at frequencies (2360 cm^{-1}) lower by a factor of 5 compared to $E \| a$ (11400 cm^{-1}). Similar results are displayed in Figure 6. They conclude a dimensional crossover from a one-dimensional to a two-dimensional metal as the temperature is lowered. The transverse coupling becomes effective below 100 K, while the smearing of the Fermi-Dirac function exceeds the transverse bandwidth of approximately $W_{b'} = 13$ meV. These conclusions are in perfect agreement with transport measurements along all three directions [58, 59] where a crossover from two-dimensional Fermi-liquid to a one-dimensional Luttinger liquid behavior was identified around $T \approx 100$ K (Figure 7). At exactly the same temperature, the c^*-axis transport turns from an insulating to a metallic one; the systems are actually three-dimensional metals at low temperatures. Jacobsen et al. made similar observation on the optical properties of (TMTSF)$_2$AsF$_6$, (TMTSF)$_2$ClO$_4$, and (TMTSF)$_2$ReO$_4$ [40, 60], where the latter compound undergoes a metal-insulator transition at $T_{AO} = 182$ K due to the anion ordering [61]. The missing plasma edge in the third direction ($E \| c^*$) [60] was later confirmed by Henderson et al. [62]. It is interesting to look at electronic band structure and how it changes with pressure [63]: the bands dispersion along the b-direction varies most, while basically no change is seen for the c-axis. This is in perfect agreement with the increasing plasma frequency observed perpendicular to the stacks.

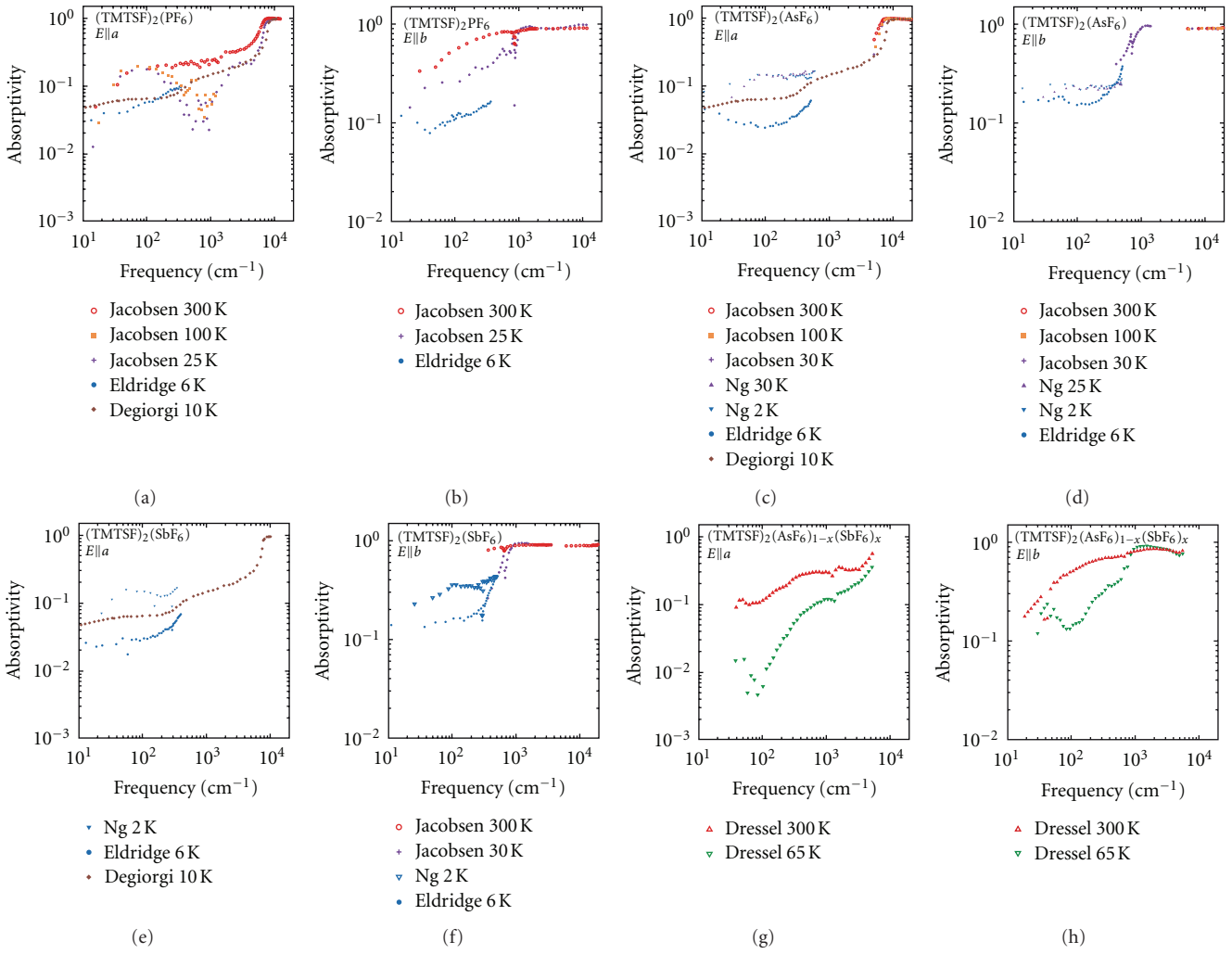

FIGURE 5: Overview of the frequency-dependent absorption $A(\omega) = 1 - R(\omega)$ of various Bechgaard salts containing octahedral anions along ($E\|a$) and perpendicular to the stacks ($E\|b'$). The results of different groups are compared in order to show the similarities in the overall behavior, but also the distinct and substantial differences. The data of $(TMTSF)_2PF_6$ are taken from Jacobsen et al. [3, 40], Eldridge et al. [41], and collaborators [42–44] at temperatures as indicated. The data of $(TMTSF)_2AsF_6$ are taken from Jacobsen et al. [40], Ng et al. [45], Eldridge and Bates [46], and Schwartz et al. [47] at temperatures as indicated. The results on $(TMTSF)_2SbF_6$ were obtained by Jacobsen et al. [40], Ng et al. [48] Eldridge and Bates [46], and Degiorgi at temperatures as indicated. The measurements on $(TMTSF)_2(AsF_6)_{1-x}(SbF_6)_x$ ($x \approx 0.15$) probe the effect of impurities on the electrodynamic response [49].

The issue of the dimensional crossover was finally explored in more detail by pressure and temperature-dependent optical investigation of $(TMTSF)_2PF_6$, $(TMTTF)_2PF_6$, and $(TMTTF)_2AsF_6$ [64–66]. The pressure-induced deconfinement transition in the Mott insulator $(TMTTF)_2PF_6$ occurs at approximately 2 GPa. This critical pressure is basically temperature independent and characterized by the rapid onset of the interstack electronic transport (along the b' direction). In Figure 8, the transverse hopping integral t_b is depicted as a function of pressure, calculated from the transverse optical conductivity ($E\|b'$)via

$$t_b^2 = \frac{\pi \epsilon_0 \hbar^2 V_c t_a \omega_p^2}{4e^2 b^2}, \quad (1)$$

where V_c denotes the unit cell volume, b the separation of the stacks, and t_a the transfer integral along the stacks. The values of t_b for $(TMTTF)_2PF_6$ and $(TMTSF)_2PF_6$ perfectly agree with each other, taking into account a pressure offset of 3 GPa between these compounds. Above the deconfinement transition (i.e., $P > 2$ GPa) and up to 4 GPa, the increase in t_b for $(TMTTF)_2PF_6$ is almost linear with a slope of 5 meV/GPa, in accord with our earlier results for $(TMTTF)_2AsF_6$ [64, 65]. Above 4 GPa the pressure-induced increase in t_b becomes weaker (~2 meV/GPa) for $(TMTTF)_2PF_6$ and comparable to the low-pressure behavior of $(TMTSF)_2PF_6$. The quantitative criterion $\Delta_\rho \approx 2t_b^*$ for the deconfinement transition [67] can be verified by comparing the pressure dependence of the charge gap Δ_ρ with that of $2t_b$ (Figure 8). The onset of the coherent electronic transport normal to the stacks occurs at

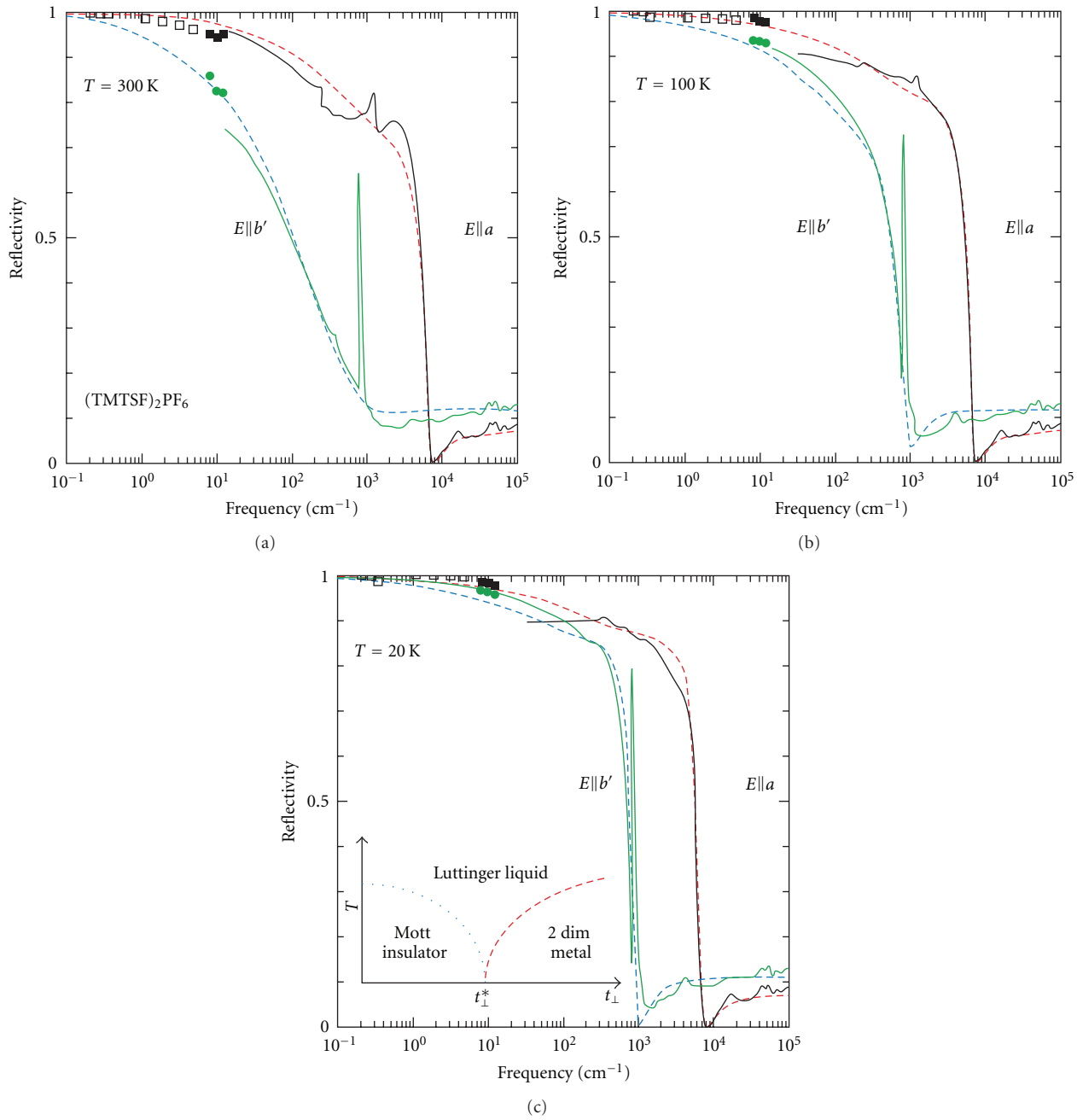

FIGURE 6: Reflectivity spectra of $(TMTSF)_2PF_6$ measured at different temperatures along the stacking axis a (solid black line) and perpendicular to it ($E\|b'$, solid green line). The filled symbols are obtained by a coherent source THz spectrometer, and the open symbols are calculated from microwave experiments [42–44, 54]. The dashed lines represent a Drude fit, respectively. The inset of panel (c) shows the schematic phase diagram of the deconfinement transition for a system of weakly coupled conducting chains as suggested by [2, 55, 56]. The transition from a Mott insulator to a two- or three-dimensional metallic state occurs at $T = 0$ when $t_\perp$ reaches a critical value $t_\perp^*$. At high enough temperature, the increase in $t_\perp$ leads to a transition from a Mott insulating to a one-dimensional Luttinger liquid and further to a dimensional crossover into a metallic state. (Figure adopted from [57]).

around 2 GPa, where $\Delta_\rho \approx 2t_b$. The size of the Mott gap, Δ_ρ, rapidly decreases as the transition point is approached and stabilizes at a finite value upon further pressure increase. These findings are in accordance with theoretical predictions [2, 55, 56, 67–72] and earlier experiments [59, 73–75] which utilized the effect of chemical pressure.

A quantitative analysis of the dimensional crossover can be obtained from the degree of coherence of the charge transport. The coherence parameter of the Drude response is given by

$$\kappa = \frac{\omega_p}{2\Gamma}, \tag{2}$$

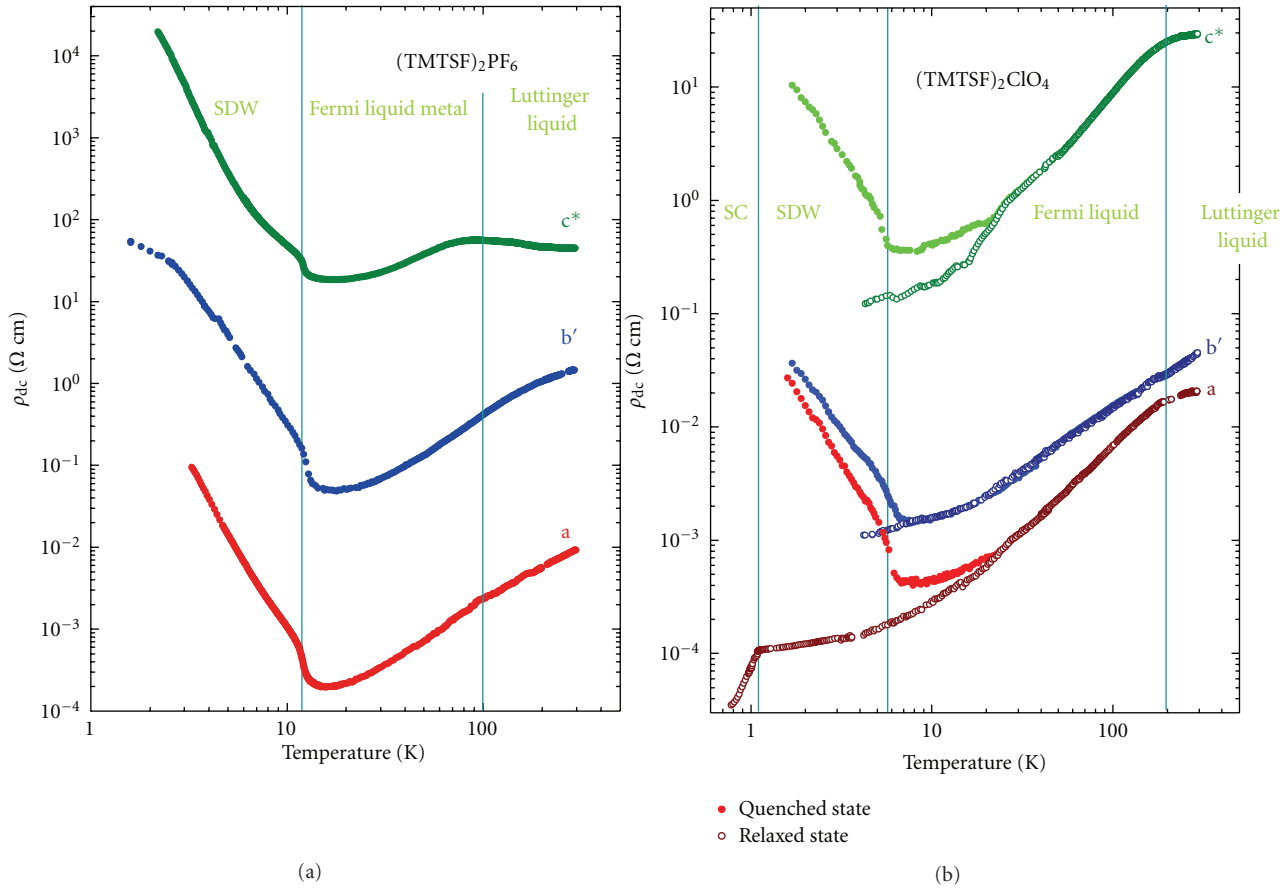

Figure 7: Temperature dependence of the dc resistivity of (a) $(TMTSF)_2PF_6$ and (b) $(TMTSF)_2ClO_4$ measured along the a (red dots), b' (blue dots), and c^* (green dots) directions (after [59]). For $(TMTSF)_2ClO_4$, the quenched and relaxed states are distinguished by solid and open circles. The ordering of the tetrahedral anions around $T_{AO} = 24\,K$ leads to a doubling of the unit cell that suppresses the spin-density-wave transition and leads to superconductivity at $T_c \approx 1\,K$. The Fermi-liquid and Luttinger-liquid regime can be distinguished by the slope in the resistivity $\rho_a(T)$ and the maximum in $\rho_c(T)$.

where ω_p and Γ are the plasma frequency and the scattering rate, respectively. Coherent transport corresponds to $\kappa > \kappa^*$, while incoherent transport occurs for $\kappa < \kappa^*$, where κ^* is a critical value of the dimensional crossover which should be close to unity.

The evolution of the dimensionality of $(TMTSF)_2PF_6$ is summarized in Figure 9(b), where the coherence parameter κ_b is plotted as a function of temperature and pressure, determined from the Drude fits of the interstack reflectivity spectra. The highest degree of coherence is achieved for high pressures and low temperatures (lower right corner of the diagrams). It gradually decreases as the pressure is released and the temperature is simultaneously raised towards the upper left corner of the diagram. The lines of constant coherence level are almost linear with pressure for $\kappa_b > 1$, however, for $\kappa_b < 1$ they become sublinear. The critical $\kappa^* = \kappa_b \simeq 0.85$ values that characterize the dimensional crossover are defined from resistivity measurements of Moser et al. [73]. The constant level line $\kappa_b \simeq 0.85$, that is, the "crossover line," is depicted in Figure 9. For pressures below 1.2 GPa, the crossover line exhibits a remarkable strong slope, not expected in the naive picture of noninteracting electrons where $T^* \propto t_b$. According to Figure 8, the interstack transfer integral t_b in $(TMTSF)_2PF_6$ increases only by about 30% when pressure increases by 4 GPa. Thus, one would expect the crossover temperature of about 130 K at 4 GPa for noninteracting electrons, in contrast to the experimental observation. This provides evidence that electronic correlations play a decisive role in the renormalization of the dimensional crossover in the Bechgaard salts, leading to the very fast suppression of the one-dimensional state in favor of a high-dimensional metallic state.

A corresponding temperature-pressure diagram of the coherence parameter κ_b is depicted in Figure 9(a) for $(TMTTF)_2PF_6$ in the deconfined state, that is, for $P > 2$ GPa. The coherence parameter demonstrates a temperature and pressure dependence similar to that of the $(TMTSF)_2PF_6$ salt. Thus, the chemical pressure offset of 3 GPa between the two studied salts in the generic phase diagram also holds for the occurrence of the dimensional crossover.

3. Mott Physics

The low-frequency properties of $(TMTSF)_2PF_6$ and $(TMTSF)_2ClO_4$ resemble features previously observed in

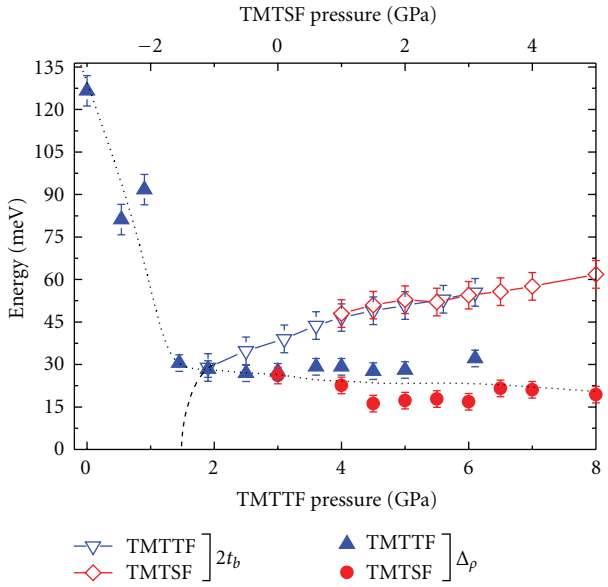

FIGURE 8: Pressure dependence of the Mott gap energy Δ_ρ (full symbols) and the transverse hopping integral $2t_b$ (open symbols) for $(TMTTF)_2PF_6$ and $(TMTSF)_2PF_6$ salts as obtained from the room-temperature data. The upper pressure scale corresponds to $(TMTSF)_2PF_6$ and is shifted by 3 GPa with respect to the lower pressure scale for the $(TMTTF)_2PF_6$ salt. The dashed line schematically indicates the vanishing of t_b at the point of the deconfinement transition (Pashkin et al. [66]).

KCP and TTF-TCNQ (cf. Section 1). From Figures 6(c) and 10, it can be seen that a strong deviation from the simple Drude behavior is observed below 1000 cm^{-1} in the reflectivity for $E\|a$; for lower frequencies $R(\omega)$ actually drops to a minimum between 50 and 100 cm^{-1} and only then rises rapidly in order to approach unity. This behavior was first observed by Jacobsen et al. [3, 40, 60, 76], later confirmed by Ng et al. [45], Degiorgi et al. [42, 43], and eventually explained by the UCLA group [44, 47] when the optical reflection experiments in the infrared spectral range could be complemented with THz measurements and microwave experiments down to 0.1 cm^{-1}.

As can be seen in Figure 11 for $(TMTSF)_2PF_6$, the frequency-dependent conductivity consisting of two distinct features: a narrow zero-energy mode at low energy containing a very small part of the spectral weight (approximately 1%) and a finite-energy mode centered around 200 cm^{-1}. Similar observations have been made for $(TMTSF)_2PF_6$, $(TMTSF)_2AsF_6$, and $(TMTSF)_2ClO_4$, as demonstrated in Figure 12. The general idea now is that these systems resemble a one-dimensional Mott system with filling slightly above one half due to internal doping as a result of the interchain coupling. The isolated stack is effectively half filled (due to the dimerization of the quarter-filled system), leading to a Mott gap Δ_ρ in the charge degrees of freedom. This is still seen in the excitation maximum around 200 cm^{-1} where the one-dimensional physics is found. The interaction between the stacks results in the Drude-like term and is solely responsible for the finite dc conductivity; here we find the higher-dimensional physics.

These are the general characteristics of a highly anisotropic interacting electron system, with either a half- or quarter-filled band. Coulomb repulsion leads to a Mott gap and, at frequencies above the effective interchain transfer integral, to a Luttinger liquid state. The finite energy feature can be described as the absorption above the Mott gap in such a one-dimensional Luttinger liquid. In particular, above the gap, the optical conductivity behaves as a power law of the frequency $\sigma(\omega) \sim (1/\omega)^\nu$, in a way characteristic of a Tomonaga-Luttinger liquid. As demonstrated in Figure 13, the exponent ν is determined experimentally to be $\nu \approx 1.3$ for $(TMTSF)_2PF_6$, $(TMTSF)_2AsF_6$, and $(TMTSF)_2ClO_4$. Comparison of the data with the Tomonaga-Luttinger theory

$$\sigma(\omega) \propto \omega^{4n^2K_\rho - 5} = \omega^\nu , \tag{3}$$

along with the value of the exponent ν suggests that the dominant mechanism responsible for the opening of the Mott gap is the quarter-filling of the band; n is the order of the commensurability, that is, electrons per site: $n = 1$ for half-filling and 2 for quarter-filling. This conclusion leads to a Luttinger liquid parameter $K_\rho \approx 0.23$, corresponding to very strong repulsion. In a general way, $K_\rho = 1$ is the noninteracting point with $K_\rho > 1$ corresponding to attraction and $K_\rho < 1$ to repulsion. The fact that the one-dimensional theory is unable to account quantitatively for the data below the high-energy peak seems to suggest that the crossover to a two-dimensional regime occurs at relatively high energies. This is in accord to the temperature-dependent resistivity displayed in Figure 7. There we observe a linear temperature dependence of the resistivity $\rho(T)$ at elevated temperatures, that crosses over to a $\rho(T) \propto T^2$ behavior at low temperatures. It is interesting that this power-law behavior extends over about an order of magnitude in temperature if the thermal contraction is properly taken into account [59].

The remaining zero-energy mode of the itinerant electrons carries only 1% of the spectral weight and shows deviations from a simple Drude response; it can be adequately described with a frequency-dependent mass and relaxation rate with quadratic frequency-dependence, suggestive of a Fermi liquid. The fact that the resistivity is dominated by electronic scattering basically up to room temperature evidences the negligible contribution of phonons. A similar conclusion is drawn from the extremely narrow zero-energy contribution, that exhibits a width of less than 1 cm^{-1} at $T = 20$ K. As mentioned above, this seems to be a general property of low-dimensional metals.

4. Spin-Density-Wave State

As can be seen from the temperature-dependent resistivity (Figures 4 and 7) of $(TMTSF)_2PF_6$, also $(TMTSF)_2AsF_6$ and $(TMTSF)_2SbF_6$, and other salts of the Bechgaard family, a spin-density-wave ground state develops at low temperature ($T_{SDW} \approx 12$ K), where the systems become insulating due to the gap in the density of states at the Fermi energy

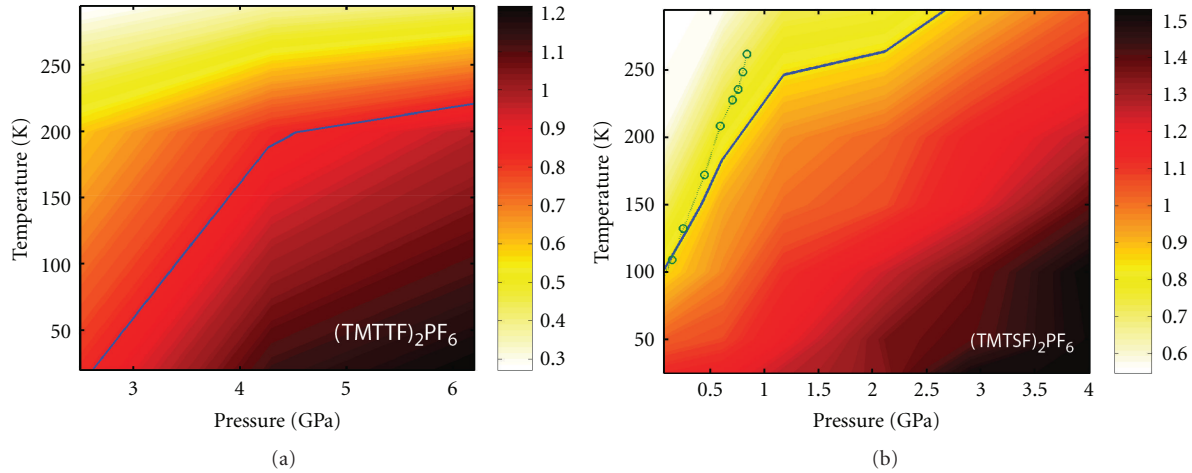

FIGURE 9: The coherence parameters of the interstack charge transport κ_b as a function of temperature and pressure for $(TMTTF)_2PF_6SF$ and $(TMTSF)_2PF_6$. The solid blue lines correspond to $\kappa_b = 0.85$. The circles illustrate the line of the dimensional crossover determined from transport measurements. The dotted line is a guide to the eye. The asterisks mark the measurement points. (after Pashkin et al. [66]).

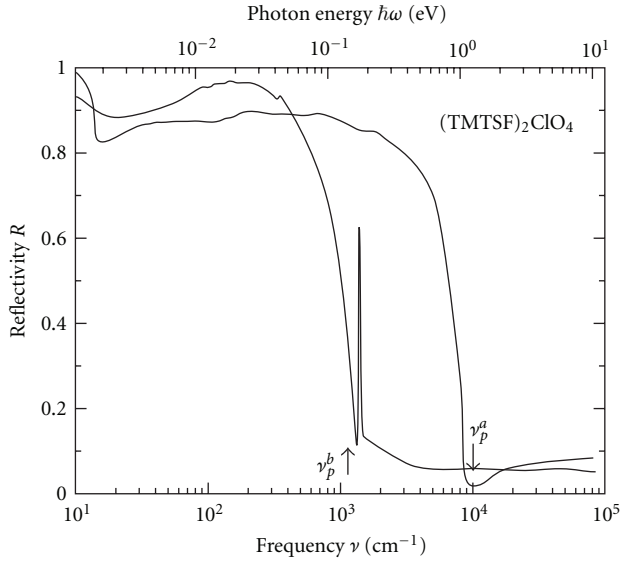

FIGURE 10: Frequency-dependence of the optical reflectivity $R(\omega)$ of $(TMTSF)_2ClO_4$ single crystals measured at $T = 10\,K$ with the electric field polarized along two different crystallographic directions a and b' (after [74]). Besides the distinctively different plasma frequencies, there are important anomalies observed at low frequencies for both directions.

that is caused by the instability of the Fermi surface due to nesting [10, 78]. The low-field dc resistivity shows an activated behavior similar to a standard semiconductor with a gap value $2\Delta/k_B \approx 45\,K$ [42, 59]. In analogy to the resistivity, the gap is expected to show up also in the optical conductivity, however, it turned out to be quite challenging to unambiguously measure the spin-density-wave gap by optical means, due to the high reflectivity, augmented by the reduced spectral weight in the relevant range of frequency.

Based on far-infrared reflection measurements on $(TMTSF)_2SbF_6$, a spin-density-wave gap of $180\,cm^{-1}$ was suggested by Ng et al. [48]; following the arguments previously developed for $(TMTSF)_2PF_6$ [79], for $T < T_{SDW} \approx 12$–$14\,K$, the semiconducting spin-density-wave state coexists with a metallic state, leading to a high conductivity background. The extracted ratio $2\Delta/k_B T_{SDW} = 18$–21 seems to be rather large. However, it is known from incommensurate Peierls transitions that the mean-field temperatures are several times the actual transition temperature due to three-dimensional ordering [78].

The Vancouver group of Eldridge tried to overcome the mentioned experimental problem by directly probing the absorptivity $A(\omega) = 1 - R(\omega)$, that is, the power absorbed by the sample [41, 46, 82]. They point out that the reflectivity of $(TMTSF)_2AsF_6$, for instance, evaluated via the directly probed absorption is almost 10% higher than previous reflection measurements on mosaics by Ng et al. [45]. Applying a novel composite-bolometric technique, the far-infrared properties of $(TMTSF)_2PF_6$, $(TMTSF)_2AsF_6$, and $(TMTSF)_2SbF_6$ were measured at low temperatures $T < T_{SDW}$. For $(TMTSF)_2PF_6$, they find a conductivity peak at $45 \pm 5\,cm^{-1}$ with a gap at $2\Delta = 33\,cm^{-1}$ that corresponds to the thermal gap Δ obtained from magnetotransport measurements by Chaikin et al. [83]. Along the chain direction ($E \| a$) an additional sharp feature was observed at $18 \pm 1\,cm^{-1}$. Interestingly for the perpendicular direction also a peak is found at $35 \pm 5\,cm^{-1}$ that also follows the $(\omega - \omega_0)^{-2}$ dependence. A gap value of $2\Delta \approx 33\,cm^{-1}$ is rather close to the mean field ratio $2\Delta/k_B T_{SDW} = 3.53$.

It was Degiorgi et al. [43] who could clearly identify the spin-density-wave gap in $(TMTSF)_2PF_6$ and later in $(TMTSF)_2ClO_4$ [77, 84] by looking in the perpendicular direction ($E \| b'$). Using a Fourier-transform spectrometer for infrared and far-infrared reflection measurements (15–$10^5\,cm^{-1}$) and a THz coherent source spectrometer for lower frequencies (7–$20\,cm^{-1}$), they probed an extremely broad spectral range. Below $T_{SDW} = 12\,K$ and $6\,K$,

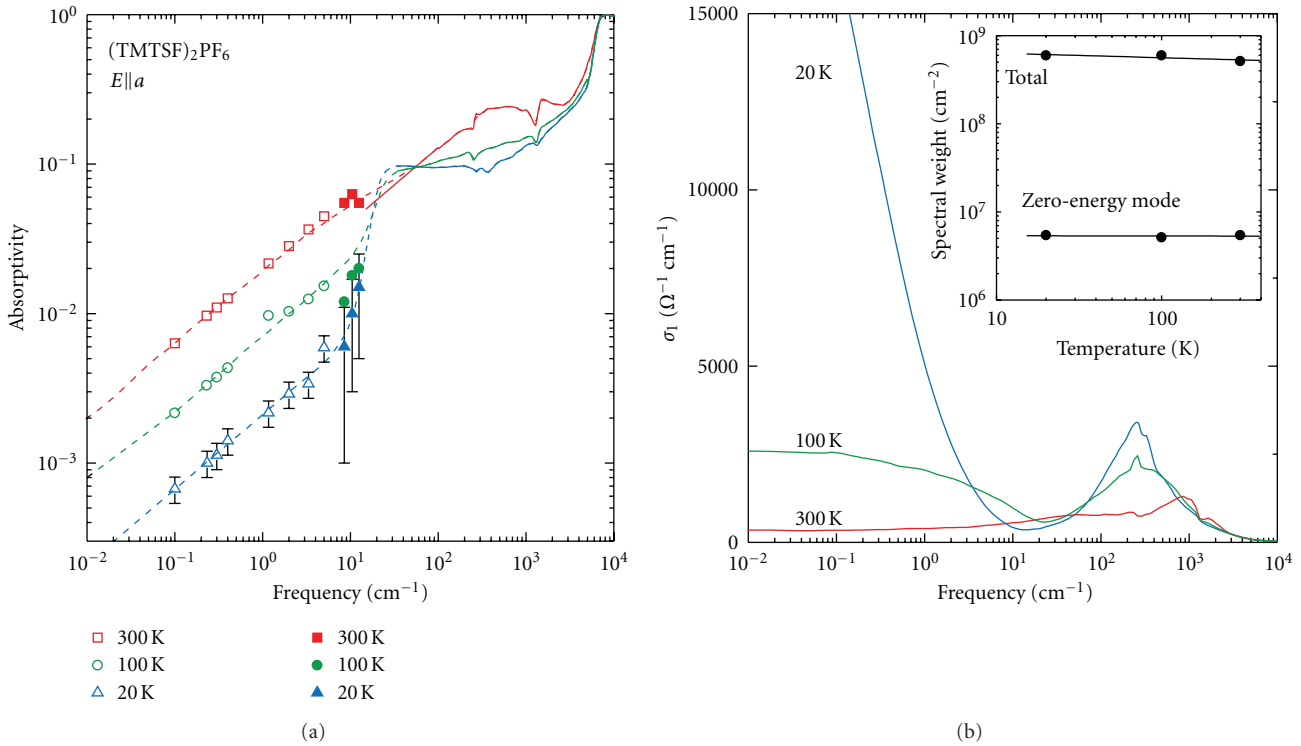

FIGURE 11: Measured (a) absorptivity $A(\omega) = 1 - R(\omega)$ and (b) conductivity $\sigma_1(\omega)$ of $(TMTSF)_2PF_6$ at 300 K, 100 K, and 20 K, for $E\|a$. The open symbols were obtained by the cavity perturbation technique. The solid symbols are from THz reflectivity measurements. The solid lines are infrared through ultraviolet reflectivity data. The dashed lines show the spectra which were used as the input for the KK calculations. The inset in (b) shows the total integrated spectral weight and the fraction in the zero-energy mode, both as functions of temperature, demonstrating that the spectral weight is not redistributed, and that only about 1% is in the Drude-like mode (after [44, 47]).

the reflectivity is significantly reduced below 70 cm^{-1} and 100 cm^{-1}, respectively, leading to an energy gap in the optical conductivity. In Figure 14, the frequency-dependent reflectivity and conductivity of $(TMTSF)_2PF_6$ is plotted for different temperatures. A gaplike feature developing at about 70 cm^{-1} for $T < T_{SDW}$, which is rather sharp, moves to slightly lower frequencies and decreases in intensity as the temperature increases. It nicely follows the mean-field behavior also extracted from magnetic measurements [85, 86]. This feature seems to persist at temperatures slightly above T_{SDW}.

Watanabe et al. measured the reflection of $(TMTSF)_2PF_6$ using a THz-time-domain spectroscopic system [87] that had sufficient resolution in phase shift to observe the transition from the metallic to the insulating spin-density-wave state. A distinct reduction of the conductivity below approximately 65 cm^{-1} gives a clear indication of the spin-density-wave gap formation in accord to [43]. In addition, they were able to investigate the photoexcited dynamics of the spin-density-wave state in $(TMTSF)_2PF_6$. After the ultrashort laser-pulse excitation (90 fs at $\lambda = 800$ nm), a metallic phase is generated within 3 ps. The sudden closing of the gap (observed in the far-infrared spectrum) is followed by a recovery of the spin-density-wave gap; the recovery time is found to diverge toward T_{SDW}, while the gap remains open at T_{SDW} [88, 89].

Compared to the two compounds discussed above, the experimental work on $(TMTSF)_2AsF_6$ and $(TMTSF)_2SbF_6$ is less substantial [48]. For $(TMTSF)_2AsF_6$, a very narrow $\Gamma = 1/(2\pi\tau c) \approx 5\,cm^{-1}$ Drude-like contribution is identified in the metallic state above the spin-density-wave transition ($T_{SDW} = 12.2$ K), that vanishes completely as $T < T_{SDW}$. Although the low-frequency conductivity ($\nu < 60\,cm^{-1}$) is slightly reduced in the spin-density-wave state (according to a decrease in reflectivity below 63 cm^{-1}), no clear evidence of a spin-density wave gap was identified [45].

The spin-density-wave ground state is characterized by a complete and more or less isotropic energy gap 2Δ in the single-particle excitation spectrum that is seen in the temperature-dependent dc resistivity $\rho(T)$ in all three directions (Figure 7). In addition, collective excitations of the many-body ground state are expected, as known from the pinned-mode resonance in the case of charge density waves. In a comprehensive series of microwave experiments, Donovan et al. [42, 90–93] succeeded to probe the frequency-dependent conductivity down to 3 GHz (corresponding to 0.1 cm^{-1}), complemented by radio frequency and standard optical experiments. As displayed in Figure 15, a Drude-like metallic behavior was found above the spin-density wave transition together with a temperature-independent feature at higher frequencies. The later one corresponds to the excitations across the Mott gap discussed above [44, 47]. A

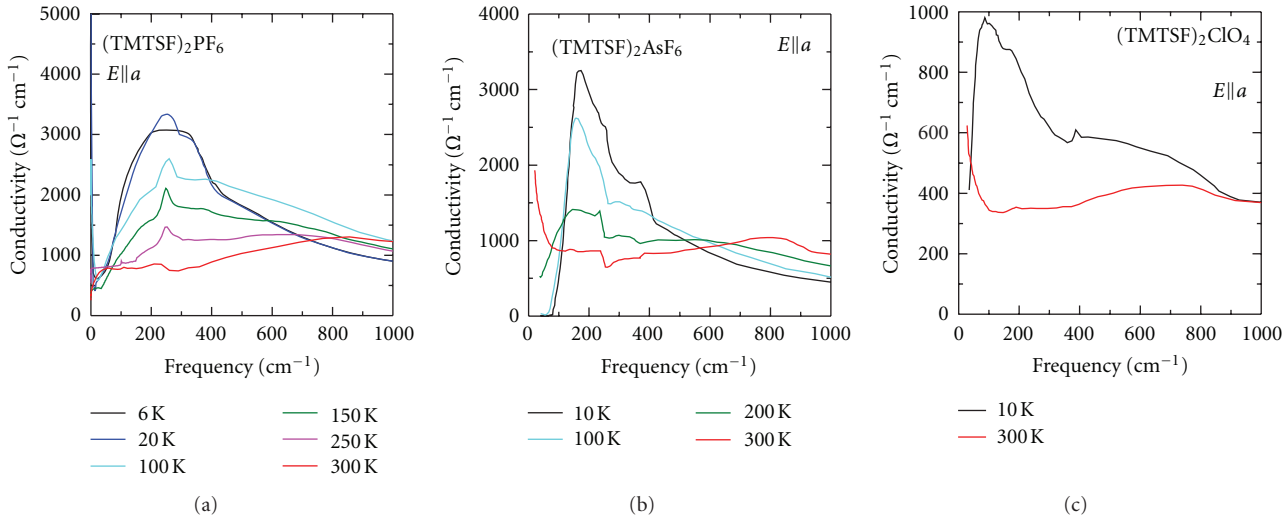

Figure 12: Optical conductivity of $(TMTSF)_2PF_6$, $(TMTSF)_2AsF_6$, and $(TMTSF)_2ClO_4$ measured along the stacking direction ($E\|a$) at different temperatures as indicated. Around 200 cm^{-1} a strong band develops which is a assigned to excitations across the Mott gap (data from [47]).

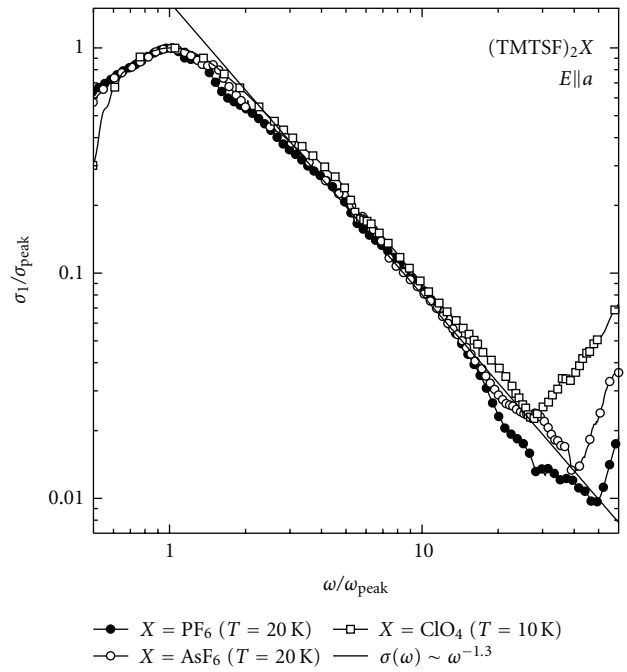

Figure 13: The normalized conductivities of $(TMTSF)_2PF_6$, $(TMTSF)_2AsF_6$, and $(TMTSF)_2ClO_4$ shown on a log-log scale to demonstrate the power law frequency-dependence of the conductivities above the finite energy peak. The solid line shows a fit of the form $\sigma(\omega) \sim \omega^{-\nu}$ with $\nu = 1.3 \pm 0.1$. (reproduced from [47]).

fit of the data by the Drude model yields a $\Gamma = 1/(2\pi c\tau) = 3\,cm^{-1}$, which places the material well into the clean limit. The ac response shows a strong frequency-dependence, and most importantly, two subgap modes can be identified: a very broad one in the radio frequency range, due to internal deformations of the spin density wave and a narrow mode near 0.1 cm^{-1}, which is interpreted as the response of the $q = 0$ phason. No evidence for a single-particle gap is seen in the infrared spectral range, but this is in full accord with a material in the clean limit. Later Petukhov and Dressel performed [94–96] microwave experiments along all three directions of the spin-density-wave model compound $(TMTSF)_2PF_6$ and could demonstrate that the pinned-mode resonance is present along the a and b axes. Since the collective transport of the spin density wave is considered to be the fingerprint of the condensate, this unambiguously proves that the density wave also slides in the perpendicular b' direction. The collective response, however, is absent along the least conducting c^* direction.

When a magnetic field of up to 10 Tesla is applied along the a axis, no change in the 16.5 GHz microwave response is observed for $(TMTSF)_2PF_6$ and $(TMTSF)_2AsF_6$ [97–99]. For $H\|c^*$ direction, however, striking changes are detected below T_{SDW} in the dielectric constant and conductivity. The local maximum near $T = 4$ K in $\sigma_1(T)$ is accompanied by a sharp decrease in $\epsilon_1(T)$; orbital effects might be important for the Fermi-surface nesting properties. This leads to changes in the behavior of the condensate. Based upon anomalies in $\epsilon_1(H, T)$ and $\sigma_1(H, T)$, an ambient pressure H-T diagram is suggested by the Sherbrooke group [98].

5. Very Low-Frequency Behavior

The discussion on the collective mode and pseudogap in one-dimensional conductors raised in the 1970 by measurements of KCP and TTF-TCNQ (cf. Section 1) was revived in the case of the Bechgaard salts. Several aspects come together are often entangled and confused; however, also the materials might not be in a well-defined ground state, but electronically phase separated between metallic, spin-density-wave and even superconducting state. It should be pointed out that the single crystals are extremely clean, with

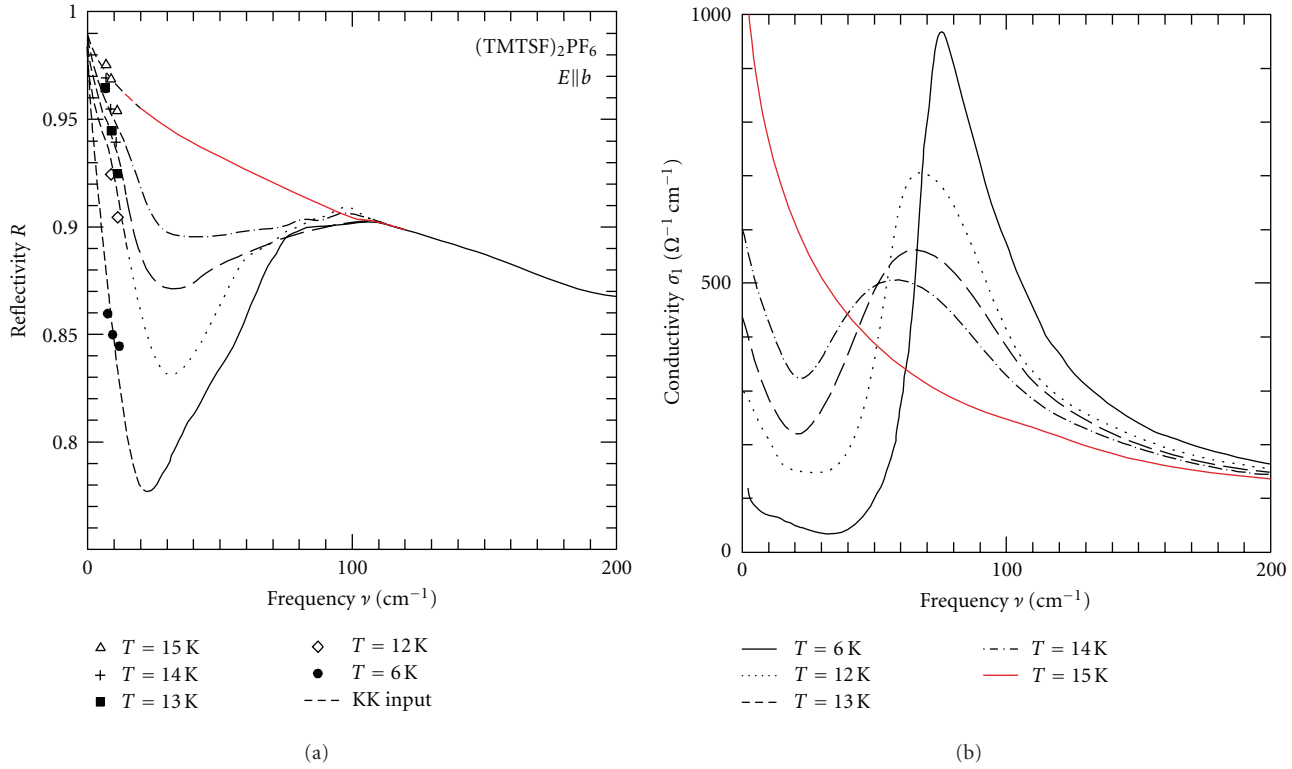

Figure 14: (a) The low-frequency optical reflectivity of $(TMTSF)_2PF_6$ measured perpendicular to the chains ($E\|b'$). The spin-density-wave gap opens as the temperature is lowered below 15 K. The solid lines are optical reflectivity data, the symbols indicate the results of the THz measurements; the dashed line represents the extrapolation for the Kramers-Kronig analysis. (b) The corresponding optical conductivity of $(TMTSF)_2PF_6$ perpendicular to the chain direction as obtained by the Kramers-Kronig transformation of the reflectivity data (after [43, 77]).

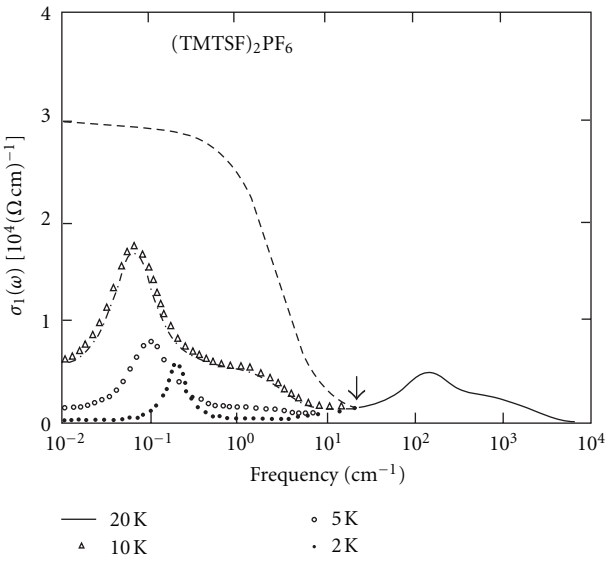

Figure 15: Frequency-dependent conductivity of $(TMTSF)_2PF_6$ measured above and below the spin-density-wave transition at $T_{SDW} = 12$ K. The single-particle gap around 30 cm^{-1} obtained from dc measurements is indicated by the arrow. The Drude-like conductivity collapses in the insulating state, but there remains a finite frequency pinned-mode resonance ascribed to the collective spin-density-wave excitation (reproduced from [42]).

a very low amount of impurities and defects. The coexistence on a microscopic scale is subject to intense investigations [100, 101]. Unfortunately, real features are also mixed with experimental artefact due to a variety of reasons, some of them discussed above. It should be noted, however, that most groups were well aware of the experimental insufficiencies and pitfalls: they present and discuss their findings with the appropriate caution. Strong claims have been rare in all those years.

Due to the ambient pressure superconductivity $(TMTSF)_2ClO_4$ has drawn most attention starting from the early days [60, 102–104] until the nice reviews of Timusk in the 1990s [80, 105, 106]. In order to allow the anions to order near 24 K, the sample has to be cooled down very slowly through T_{AO}; only then the metallic state is preserved and superconductivity reached at $T_c = 1.2$ K. Fast cooling results in the insulating spin-density-wave ground state (Figure 7(b)0. Unfortunately the actual situation for most optical experiments will be a mixture of both states, making the interpretation of the spectra difficult [107].

The challenge of the low-frequency electrodynamic properties is presented in Figure 16, following the review of Cao et al. [80]. Although the overall reflectivity obtained from various groups agrees quite well, the absolute values differ by up to 10% [80, 108]. As nicely demonstrated by Eldridge and Bates [46], an increase of $R(\omega < 100\,cm^{-1})$ by only

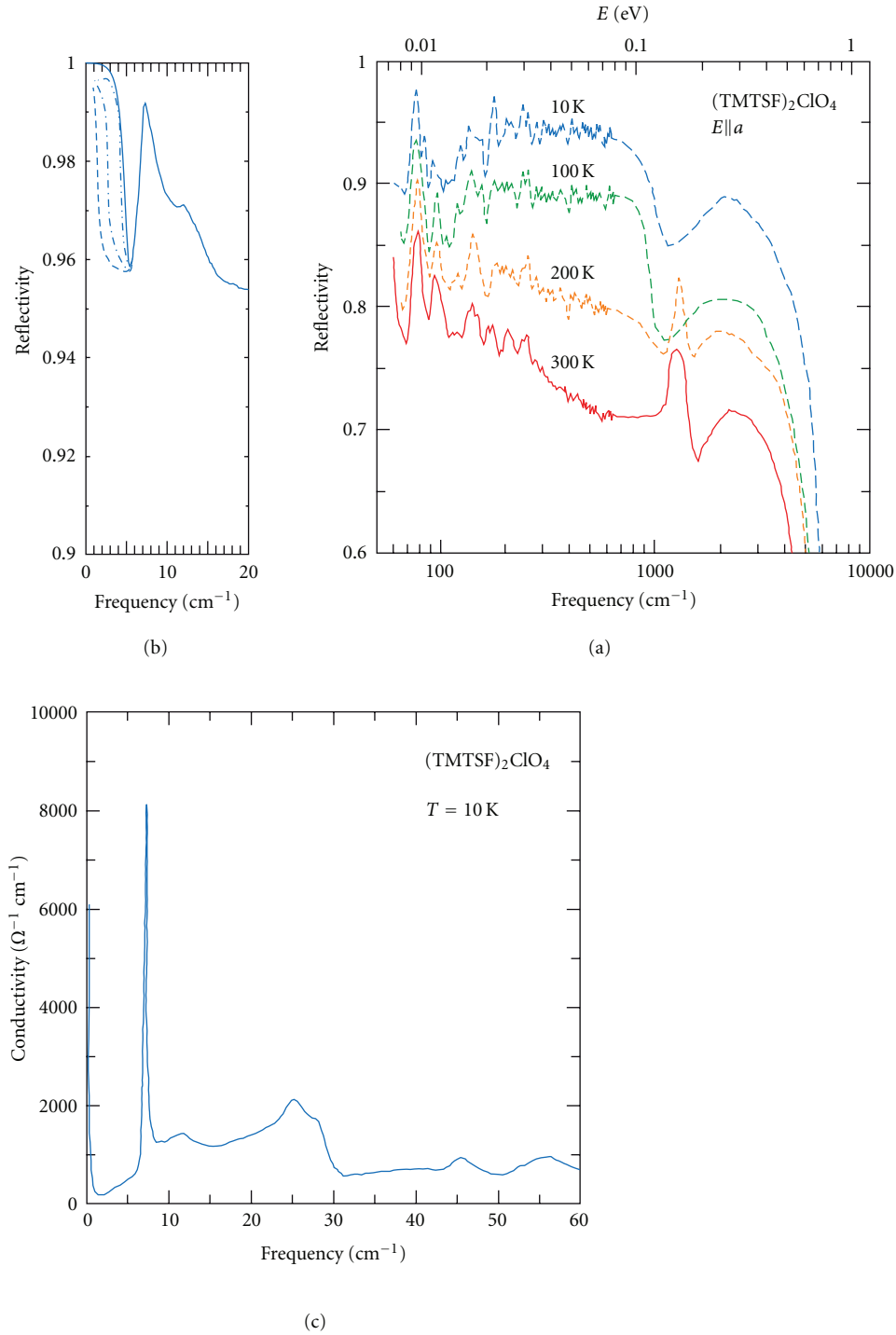

FIGURE 16: (a) Frequency-dependent reflectivity of a $(TMTSF)_2ClO_4$ mosaic measured along the a-axis at different temperatures (after [80]). (b) Low-frequency reflectivity (solid line) and the fitted low-frequency extensions (data taken from [81]). Note the different axes for both panels. The sharp plasma edge at 4 cm^{-1} is required to match the dc conductivity; alternative extrapolations are displayed by dashed lines. (c) Calculated optical conductivity of $(TMTSF)_2ClO_4$ at $T = 10$ K (after [80]).

1.5% doubles the peak height in conductivity by half the width. The lowest frequency extrapolation of the reflectivity is commonly done by a Hagen-Rubens assumption, with or without taking the actual dc conductivity into account. In Figure 16(b), different extrapolations are plotted, where the solid line corresponds to a Drude-like term with a plasma frequency of $\nu_p = \omega_p/(2\pi c) = 634\,cm^{-1}$ and a scattering rate of only 0.034 cm^{-1}. The corresponding optical conductivity obtained from a Kramers-Kronig analysis is shown in Figure 16(c). Not only the zero-frequency mode

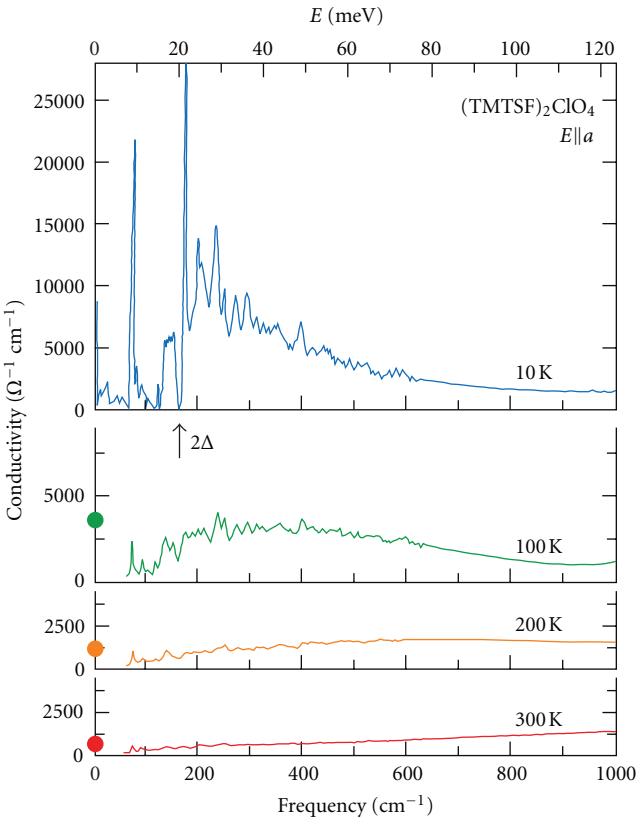

FIGURE 17: Optical conductivity of $(TMTSF)_2ClO_4$ for the longitudinal polarization $E\|a$ measured at different temperatures (after [80]). The full circles denote the values of the dc conductivity [45], where $\sigma_{dc}(10\,K) = 2 \times 10^5\,\Omega^{-1}cm^{-1}$ is above scale. A gap $2\Delta = 170\,cm^{-1}$ is evident in $\sigma_1(\omega)$ at $T = 10\,K$.

is influenced by the assumed extrapolation, but also the amplitude of the low-lying phonon line at $7\,cm^{-1}$.

As can be seen in Figures 16(c) and 17, the far-infrared optical conductivity is rather small in contrast to the dc conductivity with no sign of a Drude absorption directly visible. Instead the optical conductivity is dominated by a broadband centered around $300\,cm^{-1}$, that can be assigned to excitations across the Mott gap [47], as discussed above. An energy gap might be identified in the spectra at $2\Delta = 170\,cm^{-1}$ for $T = 10\,K$. There is an overall shift of spectral weight to lower energies as the temperature is reduced.

Challener et al. measured the far-infrared properties of $(TMTSF)_2ClO_4$ between 4 and $40\,cm^{-1}$ down to $T = 2\,K$ [109, 110]. They identified two phonon-like peaks in the reflectivity at 7 and $29\,cm^{-1}$; the upper one does not change with magnetic fields up to 4 Tesla, but vanishes upon irradiation and temperature increase to 20 K. In contrast, the McMaster group [81, 104] found this mode to be sensitive to magnetic field and thus rules out direct phonon absorption. Two far-infrared features, one at 7 and one at $25\,cm^{-1}$ seem to be robust, where the later one is suppressed as a field $B = 0.7$ Tesla is applied and shifts by $2\,cm^{-1}$ when the temperature is raised to 24 K. However, it is obvious that this feature cannot be identified with the superconducting gap nor with the spin-density-wave state [104].

It was pointed out by Eldridge et al. [111–114] that the TMTSF salts with centrosymmetric anions, such as $(TMTSF)_2ClO_4$, behave quite differently than the one with tetrahedral anions, for instance $(TMTSF)_2PF_6$, $(TMTSF)_2AsF_6$ or $(TMTSF)_2SbF_6$, since the zone folding at the anion order T_{AO} causes a sharp structure in the far-infrared spectral range. Recently a complete vibrational study was published [115] including Raman and infrared modes, intramolecular as well as lattice vibrations. The $(TMTTF)_2X$ salts crystallize in triclinic $P\bar{1}$ space, but the stack dimerization can be neglected and a pseudo-monoclinic unit cell approximated with C_{2h} symmetry [116]. In the spectral region below $200\,cm^{-1}$ at most, 15 lattice modes are expected: 6 due to the rigid translations and rotations of the anions and 9 due to the $(TMTTF)_2$ dimer degrees of freedom. The anion translations are infrared active and have A_u symmetry (translation along a-axis), and B_u symmetry (translations perpendicular to the a axis) while the three anion rotations are Raman active with one A_g and two B_g symmetry modes. When the TMTSF salts with tetrahedral anions undergo an anion order transition at T_{AO}, the unit cell is doubled in all three directions: $q = (1/2, 1/2, 1/2)$ [117]; implying that the there are eight times as many phonons present below T_{AO}. Eldridge et al. interpret the $30\,cm^{-1}$ feature—that actually exists already above the anion order T_{AO} as a very broadband in their powder absorption spectra—as a transverse acoustic zone-boundary phonon which is coupled very strongly with the electrons [111]. Note, however, that Ng et al. [81] found this phonon mode to be sensitive to magnetic field in $(TMTSF)_2ClO_4$, although not confirmed by the Richards' group [109]. By extending the experiments up to magnetic fields of 20 Tesla, Janssen et al. confirmed that this zone-folding phonon mode actually couples to the field-induced spin-density-wave state [118].

These far-infrared spectroscopic measurements (in reflection and transmission mode) in very high magnetic fields ($B < 20$ Tesla and $T = 0.4\,K$) made it possible to explore the field-induced spin-density-wave states. Perel et al. [119] identified a spin-density-wave gap at $12\,cm^{-1}$ from their reflection measurements at $T = 1.2\,K$, slightly lower than the one reported by Janssen et al.. A partial gap around $14\,cm^{-1}$ is most pronounced in all field-induced spin-density-wave phases. Two sharp features appear around 17 and $32\,cm^{-1}$, and a smaller one at $23\,cm^{-1}$; none of them shift with magnetic field. A peak shows up at $2.4\,cm^{-1}$ that becomes stronger with increasing field and is thought to be a collective mode excitation [118], although its eigenfrequency is considerably lower than the pinned-mode resonance observed by the UCLA group [42, 90].

In order to probe the superconducting state Reedyk and collaborators [120] measured the low-temperature reflectivity ($E\|a$) of $(TMTSF)_2ClO_4$ in the spectral range from 10–$70\,cm^{-1}$ down to 0.45 K. When $T < T_c$ they find a shift of the low-frequency reflectivity step (associated to the plasma edge of the Drude contribution) to higher frequencies. Also the $30\,cm^{-1}$ mode exhibits an upward shift by about

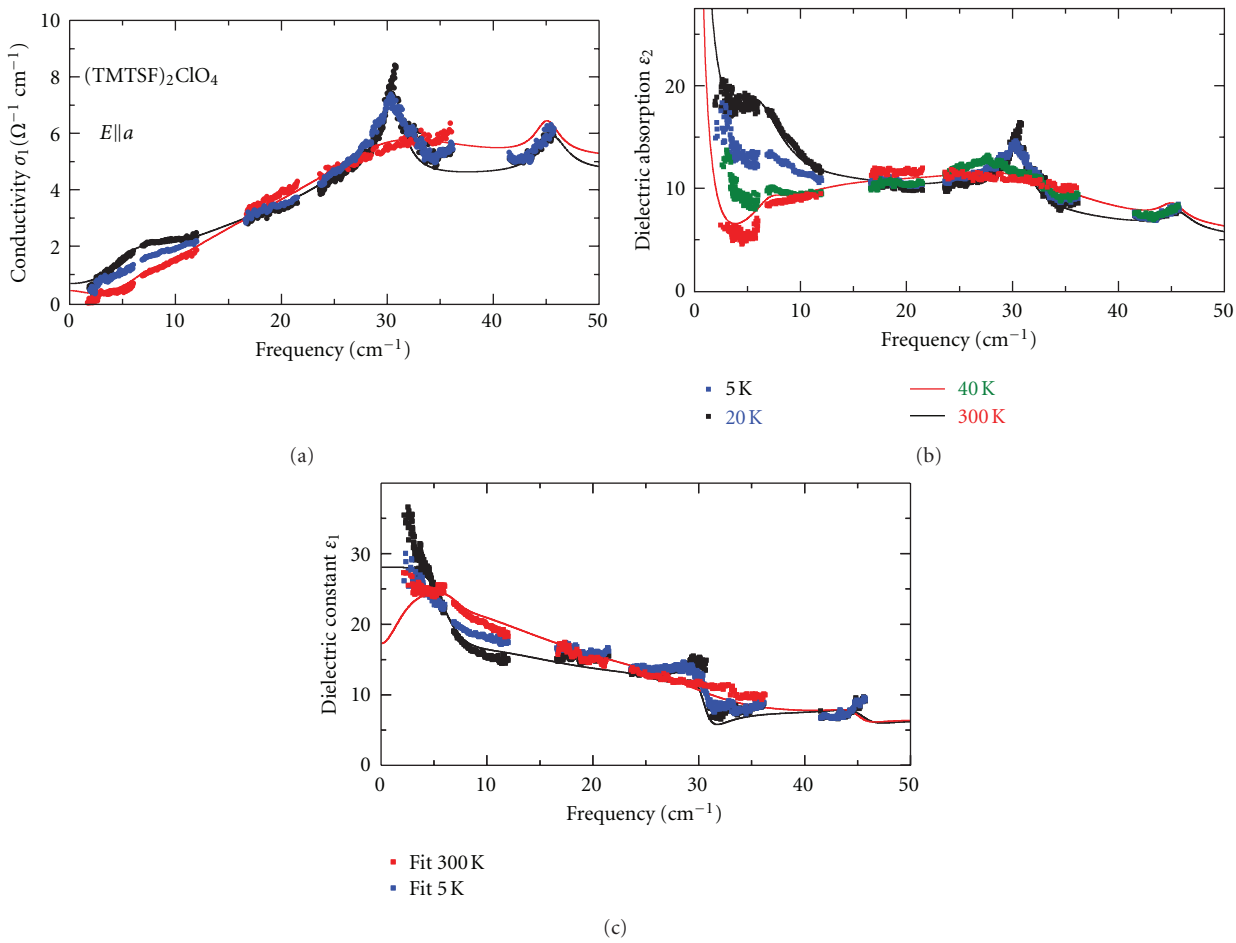

FIGURE 18: (a) Optical conductivity $\sigma_1(\omega)$ of $(TMTSF)_2ClO_4$ obtained from powder transmission measurements at different temperatures as indicated. (b) Corresponding imaginary part of the dielectric constant $\epsilon_2(\omega)$, describing the absorption and (c) real part of the dielectric constant $\epsilon_1(\omega)$.

$2\,\mathrm{cm}^{-1}$. These observations are interpreted as coupling to quasiparticle excitations across the superconducting gap. As already pointed out previously [104], no direct evidence of the superconducting energy gap can be found in optical experiments.

In Figure 18, recent transmission measurements are presented for the spectral range from 1.6 to $46\,\mathrm{cm}^{-1}$ [121] obtained by employing a coherent source THz spectrometer [16]. In order to avoid the well-known difficulties with the high reflection values, the sample surface and problems due to mosaic sample, finely ground $(TMTSF)_2ClO_4$ crystals were dispersed in an appropriate oil and pressed in free-standing pellets. Although this procedure mixes the different crystallographic directions and causes uncertainties in the absolute values, it is free of spurious peaks due to diffraction and leakage. The sample was cooled by approximately 0.8 K per min in the temperature range from $T = 300\,\mathrm{K}$ down to 5 K in order to arrive at the relaxed metallic state. At low temperatures, we can clearly identify a peak in the conductivity centered around $30\,\mathrm{cm}^{-1}$ and a smaller mode at $7\,\mathrm{cm}^{-1}$. In addition, there always remains a Drude-like contribution necessary to describe the metallic conductivity. In Figure 19, the temperature dependences of those parameters are plotted that were used to fit these three contributions. The static conductivity $\sigma_1(\omega \rightarrow 0)$ obtained from a zero-frequency extrapolation corresponds to a mixture of all three crystallographic directions and thus cannot be simply compared to direct four-probe dc measurements (Figure 4). If we confine ourselves to the optical data, we obtain $1/(2\pi\tau c) \approx 2$–$10\,\mathrm{cm}^{-1}$, as plotted in Figure 19(b), which is different than the very narrow Drude-like contribution as previously discussed by Timusk et al. [80, 81] for the results for $E\|a$. They used values of $1/(2\pi\tau c) \approx 0.03\,\mathrm{cm}^{-1}$, in order to fit the dc conductivity along the chains and suggest even smaller one (Figure 16(b)). It is interesting to note, that the dielectric constant is still positive and increases as the frequency is reduced, indicating the dominance of the least-conducting direction and a gaplike feature.

Part of it comes from the low-frequency mode seen around $7\,\mathrm{cm}^{-1}$. It was already discovered by several groups three decades ago [81, 109], without a clear assignment. The fit by a Lorentzian line is not really satisfactory, implying that it might reflect a gaplike feature. From the temperature dependence of its spectral weight displayed in Figure 19(c),

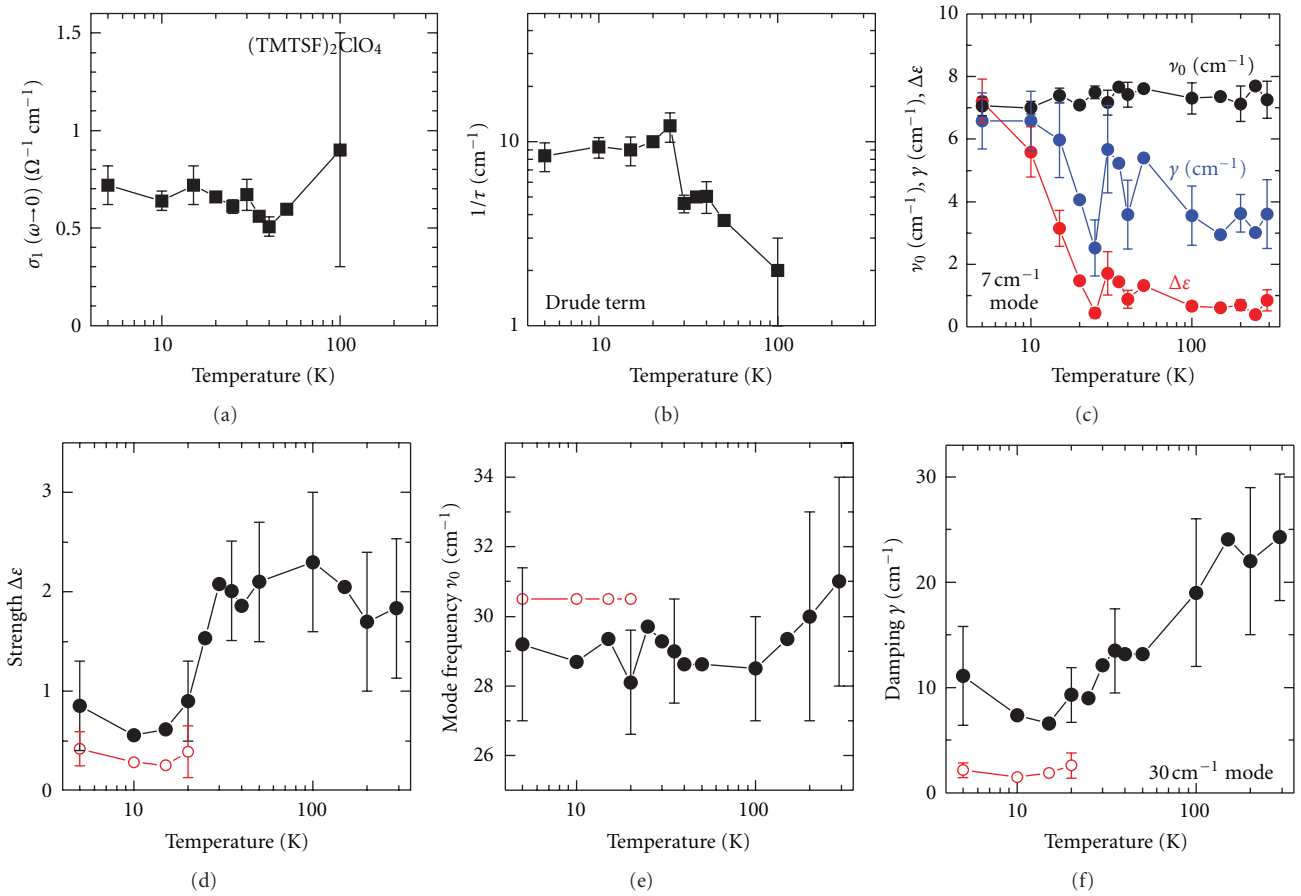

Figure 19: Temperature dependence of the mode parameters obtained from fitting the optical properties of $(TMTSF)_2ClO_4$ obtained from powder transmission measurements. (a) Zero-frequency conductivity $\sigma_1(\omega \to 0)$ and (b) scattering rate of the Drude contribution to the optical conductivity of $(TMTSF)_2ClO_4$. (c) Parameters of the mode that develop around 7 cm^{-1}: ν_0 denotes the eigenfrequency, γ the width, and $\Delta\epsilon$ the mode strength (spectral weight). Temperature dependence of the parameters of the 30 cm^{-1} mode: (d) the spectral weight given as a mode strength $\Delta\epsilon$, (e) the center frequency ν_0, and (f) the damping γ of the mode. The lines connect the data points. The open symbols correspond to a second mode that has to be introduced at slightly higher frequencies for a complete description.

we see a strong increase of strength below 20 K, which infers a connection to the anion order at $T_{AO} = 24$ K rather than to spin-density-wave state that develops in the quenched state only below 7 K and should not be present in our sample. It should be noted here that a similar mode is not observed for centrosymmetric anions (Figure 21). This supports our assignment to an acoustic phonon mode that becomes activated by the back-folding of the Brillouin zone below T_{AO}.

Most pronounced in the $(TMTSF)_2ClO_4$ spectra (Figure 18) is the strong mode at 30 cm^{-1} that can be identified up to elevated temperatures but strongly decreases its width (Figure 19(f)). Below $T \leq 20$ K a second peak seems to appear close by and a satisfactory fit can only be obtained by introducing an additional Lorentz term, indicated by the open symbols in Figures 19(d)–19(f). The constant frequency and decreasing line width presented in Figure 19(f) confirm previous findings by Eldridge et al. [111], also based on powder transmission measurements in the far-infrared. Finding similar modes in other Bechgaard salts with octahedral anions, such as $(TMTSF)_2BF_4$ and $(TMTSF)_2ReO_4$, makes them conclude that this feature has to be assigned to a transverse-acoustic zone-boundary phonon that couples strongly with the electrons.

Applying their novel composite-bolometric technique to various Bechgaard salts, the far-infrared properties of $(TMTSF)_2PF_6$, $(TMTSF)_2AsF_6$, and $(TMTSF)_2SbF_6$ were measured by the UBC group [41, 46, 82] at low temperatures $T < T_{SDW}$. For $(TMTSF)_2PF_6$, they find a conductivity peak at 45 ± 5 cm^{-1} with a gap at $2\Delta = 33$ cm^{-1} that corresponds to the thermal gap Δ obtained from magnetotransport measurements by Chaikin et al. [83]. Along the chain direction ($E \| a$) an additional sharp feature was observed at 18 ± 1 cm^{-1}. Interestingly for the perpendicular direction a peak is found at 35 ± 5 cm^{-1} that also follows the $(\omega - \omega_0)^{-2}$ dependence.

In Figure 20, the low-temperature ($T = 5$ K) optical transmission of $(TMTSF)_2PF_6$ is shown for the extremely low-frequency range spanning from 1.6 to 12.6 cm^{-1}. The experiments are performed on a large number of ground

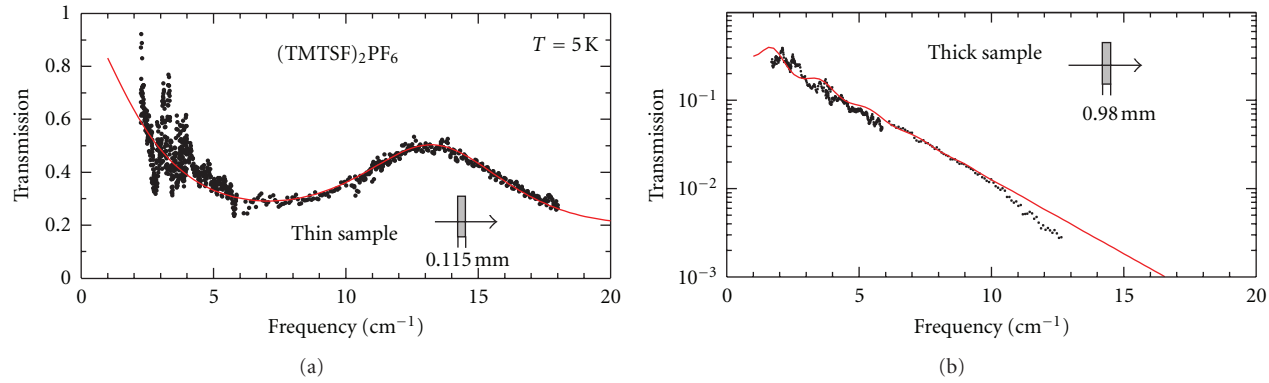

FIGURE 20: Transmission spectra through $(TMTSF)_2PF_6$ powder dispersed in oil. The spectra were taken at $T = 5\,K$. The red solid lines correspond to a fits using Fresnel's equations. (a) Transmission coefficient through a thin sample of $d = 0.115\,mm$. Interference within the pressed pellet yields the maximum at $13\,cm^{-1}$. The strong scattering of the data below $5\,cm^{-1}$ is a result of standing waves within the cryostat windows. (b) Transmission coefficient through a film with thickness $d = 0.98\,mm$. The data are more accurate at low frequencies.

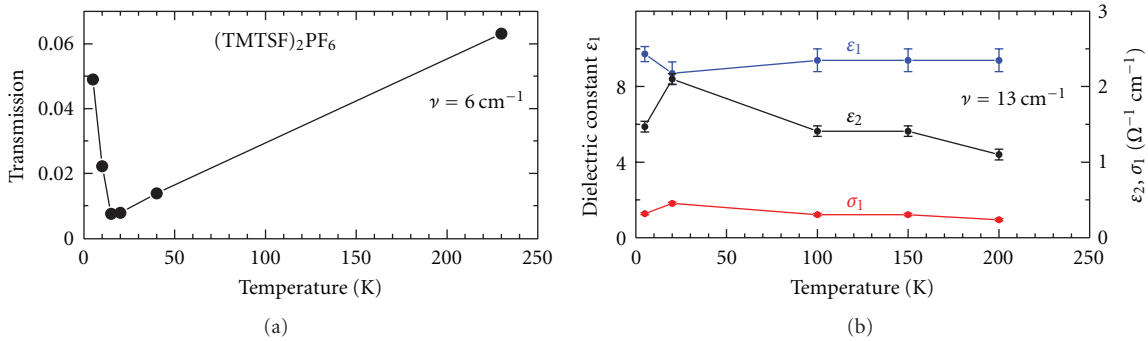

FIGURE 21: Optical properties of $(TMTSF)_2PF_6$ as a function of temperature obtained from the pressed-powder transmission measurements displayed in Figure 20. (a) Temperature-dependent transmission coefficient measured through the $d = 0.98\,mm$ sample at $\nu = 6\,cm^{-1}$. (b) Dielectric constant ϵ_1 (left scale), dielectric absorption ϵ_2 and optical conductivity σ_1 (right axis) measured at $\nu = 13\,cm^{-1}$ at different temperatures. The lines connect the data points.

crystals pressed into pellets of different thickness ($d = 0.98\,mm$ and $0.115\,mm$) in order to optimize the transmission for low and high frequencies. In the thin sample Fabry-Pérot interferences are present due to the multireflection within the pellet. These are strongly damped for the thick sample. Analyzing the spectra at different temperatures with Fresnel's equations [10, 16], we obtain the conductivity $\sigma_1(\omega, T)$ and dielectric constant $\epsilon_1(\omega, T)$ as a function of frequencies for various temperatures. As an example, the temperature-dependent parameters are plotted in Figure 21. According to the metallic behavior, the low-frequency transmission ($\nu = 6\,cm^{-1}$) strongly decreases as the temperature is reduced down to the spin-density-wave transition at $T_{SDW} = 12\,K$; in the insulating state, the transmission rapidly increases (Figure 21(a)). As seen from the overview of Figure 11, at $\nu = 6\,cm^{-1}$ we still probe the Drude-like contribution that collapses at the metal-to-insulator transition. In Figure 21(b), we consider the parameters right between the Drude term and the band assigned to the excitations across the Mott gap. As the temperature is lowered, there is only a minor variation of $\sigma_1(T)$ around T_{SDW}, that is also seen in the dielectric constant. This implies that the change in spectral weight is small due to the spin-density-wave transition.

6. Outlook

After 30 years of enormous efforts from various groups all around the globe, the low-frequency properties of one-dimensional conductors remain a challenge with many open questions. In particular, the GHz and THz range is still unexplored, except some isolated points obtained from the cavity perturbation method. What is the width of the zero-frequency mode? Does it exhibit a Drude shape, or does the scattering rate follow a ω^2 dependence expected for a Fermi liquid? What is the development with temperature? Is the spectral weight conserved? Up to which frequency the spectrum is involved in a redistribution with temperature? How does the reduced spectral density observed in photoemission experiments reflect in the optical data? Can we probe the superconducting gap by optical means? Is there a coexistence of the collective excitations of the spin-density-wave and superconducting ground state? Hopefully it will not take another 30 years to clarify these issues.

Acknowledgments

Important contributions of L. Degiorgi, S. Donovan, B. Gorshunov, G. Grüner, S. Kaiser, T. Knoblauch, C. Kuntscher, M. Masino, A. Pashkin, K. Petukhov, E. Rose, B. Salameh, A. Schwartz, G. Untereiner, and P. Zornoza over the last decade are sincerely acknowledged. The project was supported by the Deutsche Forschungsgemeinschaft (DFG).

References

[1] E. H. Lieb and D. C. Mattis, Eds., *Mathematical Physics in One Dimension*, Academic Press, New York, NY, USA, 1966.

[2] T. Giamarchi, *Quantum Physics in One Dimen-Sion*, Oxford University Press, Oxford, UK, 2004.

[3] C. S. Jacobsen, D. B. Tanner, and K. Bechgaard, "Dimensionality crossover in the organic superconductor tetramethyltetraselenafulvalene hexafluorophosphate $[(TMTSF)_2PF_6]$," *Physical Review Letters*, vol. 46, no. 17, pp. 1142–1145, 1981.

[4] P. Brüuesch, "Optical properties of the one-dimensional Pt complex compounds," in *One-Dimensional Conductors*, H. G. Schuster, Ed., p. 194, Springer, Berlin, Germany, 1975.

[5] P. Brüesch, S. Strässler, and H. R. Zeller, "Fluctuations and order in a one-dimensional system. A spectroscopical study of the Peierls transition in $K_2[Pt(CN)_4]Br_{0.03} \cdot 3H_2O$," *Physical Review B*, vol. 12, no. 1, pp. 219–225, 1975.

[6] H. Basista, D. A. Bonn, T. Timusk, J. Voit, D. Jérome, and K. Bechgaard, "Far-infrared optical properties of tetrathiofulvalene-tetracyanoquinodimethane (TTF-TCNQ)," *Physical Review B*, vol. 42, no. 7, pp. 4088–4099, 1990.

[7] S. Kagoshima, H. Nagasawa, and T. Sambongi, *One-Dimensional Conductors*, vol. 72 of *Springer Series in Solid-State Sciences*, Spinger, Berlin, Germany, 1989.

[8] H. R. Zeller, "Electronic properties of one-dimensional solid state systems," in *Festkörperprobleme (Advances in Solid State Physics)*, H. J. Queisser, Ed., vol. 13, p. 31, Pergamon Press, New York, NY, USA, 1973.

[9] H. R. Zeller, "Electrical transport and spectroscopical studies of the Peierls transition$K_2[Pt(CN)_4]Br_{0.03} \cdot 3H_2O$," in *Low Dimensional Cooperative Phenomena*, H. J. Keller, Ed., pp. 215–233, Plenum Press, New York, NY, USA, 1975.

[10] M. Dressel and G. Grüner, *Electrodynamics of Solids*, Cambridge University Press, Cambridge, UK, 2002.

[11] O. Klein, S. Donovan, M. Dressel, and G. Grüner, "Microwave cavity perturbation technique: part I: principles," *International Journal of Infrared and Millimeter Waves*, vol. 14, no. 12, pp. 2423–2457, 1993.

[12] S. Donovan, O. Klein, M. Dressel, K. Holczer, and G. Grüner, "Microwave cavity perturbation technique: part II: experimental scheme," *International Journal of Infrared and Millimeter Waves*, vol. 14, no. 12, pp. 2459–2487, 1993.

[13] M. Dressel, S. Donovan, O. Klein, and G. Grüner, "Microwave cavity perturbation technique: part III: applications," *International Journal of Infrared and Millimeter Waves*, vol. 14, no. 12, pp. 2489–2517, 1993.

[14] A. Schwartz, M. Dressel, A. Blank et al., "Resonant techniques for studying the complex electrodynamic response of conducting solids in the millimeter and submillimeter wave spectral range," *Review of Scientific Instruments*, vol. 66, no. 4, pp. 2943–2953, 1995.

[15] M. Dressel, O. Klein, S. Donovan, and G. Grüner, "High frequency resonant techniques for studying the complex electrodynamic response in solids," *Ferroelectrics*, vol. 176, no. 1–4, pp. 285–308, 1996.

[16] B. P. Gorshunov, A. Volkov, I. E. Spektor et al., "Terahertz BWO-spectrosopy," *International Journal of Infrared and Millimeter Waves*, vol. 26, no. 9, pp. 1217–1240, 2005.

[17] L. B. Coleman, M. J. Cohen, D. J. Sandman, F. G. Yamagishi, A. F. Garito, and A. J. Heeger, "Superconducting fluctuations and the peierls instability in an organic solid," *Solid State Communications*, vol. 12, no. 11, pp. 1125–1132, 1973.

[18] M. J. Cohen, L. B. Coleman, A. F. Garito, and A. J. Heeger, "Electrical conductivity of tetrathiofulvalinium tetracyanoquinodimethan (TTF) (TCNQ)," *Physical Review B*, vol. 10, no. 4, pp. 1298–1307, 1974.

[19] D. Jérome and H. J. Schulz, "Organic conductors and superconductors," *Advances in Physics*, vol. 31, no. 4, pp. 299–490, 1982.

[20] L. B. Coleman, C. R. Fincher, A . F. Garito, and A. J. Heeger, "Far-infrared single crystal studies of TTF-TCNQ," *Physica Status Solidi (b)*, vol. 75, no. 1, pp. 239–246, 1976.

[21] M. J. Cohen, L. B. Coleman, A. F. Garito, and A. J. Heeger, "Electronic properties of tetrathiafulvalenium-tetracyanoquinodimethanide (TTF-TCNQ)," *Physical Review B*, vol. 13, no. 11, pp. 5111–5116, 1976.

[22] G. A. Thomas, D. E. Schafer, F. Wudl et al., "Electrical conductivity of tetrathiafulvalenium-tetracyanoquinodimethanide (TTF-TCNQ)," *Physical Review B*, vol. 13, no. 11, pp. 5105–5110, 1976.

[23] D. B. Tanner, C. S. Jacobsen, A. F. Garito, and A. J. Heeger, "Infrared conductivity of tetrathiofulvalene tetracyanoquinodimethane (TTF- TCNQ) films," *Physical Review Letters*, vol. 32, no. 23, pp. 1301–1305, 1974.

[24] C. S. Jacobsen, D. B. Tanner, and A. J. Heeger, "Single-crystal reffectance studies of tetrathiafulvalene tetracyanoquinodimethane," *Physical Review Letters*, vol. 32, pp. 1559–1562, 1974.

[25] D. B. Tanner, C. S. Jacobsen, A. F. Garito, and A. J. Heeger, "Infrared studies of the energy gap in tetrathiofulvalene-tetracyanoquinodimethane (TTF-TCNQ)," *Physical Review B*, vol. 13, no. 8, pp. 3381–3404, 1976.

[26] J. E. Eldridge and F. E. Bates, "Far-infrared optical properties of semiconducting tetrathiafulvalene tetracyanoquinodimethane (TTF-TCNQ), including the pinned charge-density wave," *Physical Review B*, vol. 28, no. 12, pp. 6972–6981, 1983.

[27] J. E. Eldridge, "Improved measurement of the far-infrared optical properties of semiconducting tetrahiafulvalene tetracyanoquinodimethane," *Physical Review B*, vol. 31, no. 8, pp. 5465–5467, 1985.

[28] D. B. Tanner, K. D. Cummings, and C. S. Jacobsen, "Far-Infrared study of the charge density wave in tetrathiafulvalene tetracyanoquinodimethane (TTF-TCNQ)," *Physical Review Letters*, vol. 47, no. 8, pp. 597–600, 1981.

[29] D. B. Tanner and C. S. Jacobsen, "Low-temperature infrared studies of TTF-TCNQ," *Molecular crystals and liquid crystals*, vol. 85, no. 1–4, pp. 137–145, 1982.

[30] B. P. Gorshunov, G. V. Kozlov, A. A. Volkov, V. Železný, J. Petzelt, and C. S. Jacobsen, "Dielectric function of TTF-TCNQ in the submillimetre range," *Solid State Communications*, vol. 60, no. 9, pp. 681–687, 1986.

[31] D. Jérome, "The physics of organic superconductors," *Science*, vol. 252, no. 5012, pp. 1509–1514, 1991.

[32] J. P. Farges, Ed., *Organic Conductors*, Marcel Dekker, New York, NY, USA, 1994.

[33] T. Ishiguro, K. Yamaji, and G. Saito, *Organic Superconductors*, Springer, Berlin, Germany, 2nd edition, 1998.

[34] N. Toyota, M. Lang, and J. M. Müller, *Low-Dimensional Molecular Metals*, vol. 154 of *Springer Series in Solid-State Science*, Springer, Berlin, Germany, 2007.

[35] A. Lebed, *The Physics of Organic Superconductors and Conductors*, vol. 110 of *Springer Series in Materials Science*, Springer, Berlin, Germany, 2008.

[36] M. Dressel, S. Kirchner, P. Hesse et al., "Charge and spin dynamics of TMTSF and TMTTF salts," *Synthetic Metals*, vol. 120, no. 1–3, pp. 719–720, 2001.

[37] M. Dressel, "Spin-charge separation in quasi one-dimensional organic conductors," *Naturwissenschaften*, vol. 90, no. 8, pp. 337–344, 2003.

[38] M. Dressel, "Ordering phenomena in quasi-one-dimensional organic conductors," *Naturwissenschaften*, vol. 94, no. 7, pp. 527–541, 2007.

[39] B. Kóhler, E. Rose, M. Dumm, G. Untereiner, and M. Dressel, "Comprehensive transport study of anisotropy and ordering phenomena in quasi-one-dimensional $(TMTTF)_2X$ salts ($X = PF_6, AsF_6, SbF_6, BF_4, ClO_4, ReO_4$)," *Physical Review B*, vol. 84, no. 3, pp. 035124-1–035124-13, 2011.

[40] C. S. Jacobsen, D. B. Tanner, and K. Bechgaard, "Optical and infrared properties of tetramethyltetraselenafulvalene $[(TMTSF)_2X]$ and tetramethyltetrathiafulvalene $[(TMTTF)_2X]$ compounds," *Physical Review B*, vol. 28, no. 12, pp. 7019–7032, 1983.

[41] J. E. Eldridge and G. S. Bates, "The far-infrared properties of $(TMTSF)_2PF_g$ and $(TMTSF)_2ClO_4$ at 6K," *Molecular Crystals and Liquid Crystals*, vol. 119, pp. 183–190, 1985.

[42] S. Donovan, Y. Kim, L. Degiorgi, M. Dressel, G. Grüner, and W. Wonneberger, "Electrodynamics of the spin-density-wave ground state: optical experiments on $(TMTSF)_2PF_6$," *Physical Review B*, vol. 49, no. 5, pp. 3363–3377, 1994.

[43] L. Degiorgi, M. Dressel, A. Schwartz, B. Alavi, and G. Grüner, "Direct observation of the spin-density-wave gap in $(TMTSF)_2PF_6$," *Physical Review Letters*, vol. 76, no. 20, pp. 3838–3841, 1996.

[44] M. Dressel, A. Schwartz, G. Grüner, and L. Degiorgi, "Deviations from drude response in low-dimensional metals: electrodynamics of the metallic state of $(TMTSF)_2PF_6$," *Physical Review Letters*, vol. 77, no. 2, pp. 398–401, 1996.

[45] H. K. Ng, T. Timusk, D. Jérome, and K. Bechgaard, "Far-infrared spectrum of di-tetramethyltetraselenafulvalene hexafluoroarsenate $[(TMTSF)_2AsF_6]$," *Physical Review B*, vol. 32, no. 12, pp. 8041–8045, 1985.

[46] J. E. Eldridge and G. S. Bates, "Far-infrared spectra of bis-(tetramethyltetraselenafulvalene) hexafluoroarsenate $[(TMTSF)_2AsF_6]$ and hexafluoroantimonate $[(TMTSF)_2SbF_6]$ in their spin-density-wave state," *Physical Review B*, vol. 34, no. 10, pp. 6992–7002, 1986.

[47] A. Schwartz, M. Dressel, G. Grüner, V. Vescoli, L. Degiorgi, and T. Giamarchi, "On-chain electrodynamics of metallic $(TMTSF)_2X$ salts: observation of Tomonaga-Luttinger liquid response," *Physical Review B*, vol. 58, no. 3, pp. 1261–1271, 1998.

[48] H. K. Ng, T. Timusk, and K. Bechgaard, "Far-infrared study of bis(tetramethyltetraselenafulvalene) hexafluoroantimonate $[(TMTSF)_2SbF_6]$: coexistence of metallic and semiconducting states," *Physical Review B*, vol. 30, no. 10, pp. 5842–5846, 1984.

[49] S. Donovan, A. Schwartz, M. Dressel et al., "Effects of anion disorder on the electrodynamical response of a spin density wave," *Ferroelectrics*, vol. 176, no. 1–4, pp. 343–352, 1996.

[50] D. Jérome, A. Mazaud, M. Ribault, and K. Bechgaard, "Superconductivity in a synthetic organic conductor $(TMTSF)_2PF_6$," *Journal de Physique Lettres*, vol. 41, no. 4, pp. L95–L98, 1980.

[51] C. S. Jacobsen, "Infrared studies on the electronic structure oforganic conductors," *Mat. Fys. Medd. Dan. Vidensk. Selsk*, vol. 41, pp. 251–290, 1985.

[52] C. S. Jacobsen, "Infrared properties of organic conductors," in *Low-Dimensional Conductors and Superconductors*, D. Jérome and L. G. Caron, Eds., vol. 155 of *NATO ASI B Series, Physics*, pp. 253–2274, Plenum Press, London, UK, 1987.

[53] C. S. Jacobsen, "Optical properties," in *Highly Conducting Quasi-One-Dimensional Organic Conductors*, E. Conwell, Ed., vol. 27 of *Semiconductors and Semimetals*, pp. 293–384, Academic Press, Boston, Mass, USA, 1988.

[54] S. Donovan, L. Degiorgi, and G. Grüner, "Electrodynamics of one-dimensional metals-optical experiments on $(TMTSF)_2PF_6$," in *Europhysics Letters*, vol. 19, pp. 433–438, 1992.

[55] S. Biermann, A. Georges, A. Lichtenstein, and T. Giamarchi, "Deconfinement transition and Luttinger to Fermi liquid crossover in quasi-one-dimensional systems," *Physical Review Letters*, vol. 87, no. 27, pp. 276405-1–276405-4, 2001.

[56] T. Giamarchi, "Theoretical framework for quasi-one dimensional systems," *Chemical Reviews*, vol. 104, no. 11, pp. 5037–5055, 2004.

[57] D. N. Basov, R. D. Averitt, D. van der Marel, M. Dressel, and K. Haule, "Electrodynamics of correlated electron materials," *Reviews of Modern Physics*, vol. 83, no. 2, pp. 471–541, 2011.

[58] C. S. Jacobsen, K. Mortensen, M. Weger, and K. Bechgaard, "Anomalous magnetoresistance in an organic conductor: $(TMTSF)_2PF_6$," *Solid State Communications*, vol. 38, no. 5, pp. 423–428, 1981.

[59] M. Dressel, K. Petukhov, B. Salameh, P. Zornoza, and T. Giamarchi, "Scaling behavior of the longitudinal and transverse transport in quasi-one-dimensional organic conductors," *Physical Review B*, vol. 71, no. 7, pp. 075104-1–075104-10, 2005.

[60] C. S. Jacobsen, D. B. Tanner, and K. Bechgaard, "Optical properties of some $(TMTSF)_2X$ compounds," *Molecular Crystals and Liquid Crystals*, vol. 79, pp. 25–38, 1982.

[61] C. S. Jacobsen, H. J. Pedersen, K. Mortensen, J. B. Torrance, and K. Bechgaard, "An unusual metal-insulator transition: bis(tetramethyltetraselenafulvalenium)-perrhenate $(TMTSF_2ReO_4)$," *Journal of Physics C*, vol. 15, no. 12, article 014, pp. 2651–2663, 1982.

[62] W. Henderson, V. Vescoli, P. Tran, L. Degiorgi, and G. Grüner, "Anisotropic electrodynamics of low dimensional metals: optical studies of $(TMTSF)_2ClO_4$," *European Physical Journal B*, vol. 11, no. 3, pp. 365–368, 1999.

[63] E. Rose, C. Loose, J. Kortus et al., "Pressure-dependent structural and electronic properties of quasi-one-dimensional $(TMTTF)_2PF_6$," *Journal of Physics*. In press.

[64] A. Pashkin, M. Dressel, and C. A. Kuntscher, "Pressure-induced deconfinement of the charge transport in the quasi-one-dimensional Mott insulator $(TMTTF)_2AsF_6$," *Physical Review B*, vol. 74, no. 16, pp. 165118-1–165118-9, 2006.

[65] A. Pashkin, M. Dressel, and C. A. Kuntscher, "Pressure-induced changes in the optical response of the quasi-1D organic salt $(TMTTF)_2AsF_6$," *Journal of Low Temperature Physics*, vol. 142, no. 3-4, pp. 563–566, 2006.

[66] A. Pashkin, M. Dressel, M. Hanfland, and C. A. Kuntscher, "Deconfinement transition and dimensional crossover in the bechgaard-fabre salts: pressure- and temperature-dependent optical investigations," *Physical Review B*, vol. 81, no. 12, pp. 125109-1–125109-11, 2010.

[67] Y. Suzumura, M. Tsuchiizu, and G. Grüner, "Confinement of interchain hopping by umklapp scattering in two coupled chains," *Physical Review B*, vol. 57, no. 24, pp. R15040–R15043, 1998.

[68] M. Tsuchiizu, Y. Suzumura, and T. Giamarchi, "Renormalized inter-chain hopping versus charge gap in two coupled chains," *Progress of Theoretical Physics*, vol. 101, no. 3, pp. 763–768, 1999.

[69] M. Tsuchiizu and Y. Suzumura, "Confinement-deconfinement transition in two coupled chains with umklapp scattering," *Physical Review B*, vol. 59, no. 19, pp. 12326–12337, 1999.

[70] M. Tsuchiizu, P. Donohue, Y. Suzumura, and T. Gia- marchi, "Commensurate-incommensurate transition in two-coupled chains of nearly half-filled electrons," *The European Physical Journal B*, vol. 19, no. 2, pp. 185–193, 2001.

[71] K. le Hur, "Weakly coupled Hubbard chains at half-filling and confinement," *Physical Review B*, vol. 63, no. 16, pp. 165110-1–165110-11, 2001.

[72] T. Giamarchi, "From luttinger to fermi liquids in organic conductors," in *The Physics of Organic Superconductors and Conductors*, pp. 719–7743, Springer, Berlin, Germany, 2008.

[73] J. Moser, M. Gabay, P. Auban-Senzier, D. Jérome, K. Bechgaard, and J. M. Fabre, "Transverse transport in $(TM)_2X$ organic conductors: possible evidence for a Luttinger liquid," *European Physical Journal B*, vol. 1, no. 1, pp. 39–46, 1998.

[74] V. Vescoli, L. Degiorgi, W. Henderson, G. Grüner, K. P. Starkey, and L. K. Montgomery, "Dimensionality-driven insulator-to-metal transition in the Bechgaard salts," *Science*, vol. 281, no. 5380, pp. 1181–1184, 1998.

[75] P. Auban-Senzier, D. Jérome, C. Carcel, and J. M. Fabre, "Longitudinal and transverse transport of the quasi-one dimensional organic conductor $TMTTF_2PF_6$ studied under high pressure," *Journal de Physique*, vol. 114, pp. 41–44, 2004.

[76] C. S. Jacobsen, D. B. Tanner, and K. Bechgaard, "In-frared and optical properties of $(TMTSF)_2X$," *Journal de Physique*, vol. 44, pp. C3-859–C3-865, 1983.

[77] V. Vescoli, L. Degiorgi, M. Dressel et al., "Spin-density-wave gap in the Bechgaard salts $(TMTSF)_2X$," *Physical Review B*, vol. 60, no. 11, pp. 8019–8027, 1999.

[78] G. Grüner, *Density Waves in Solids*, Addison-Wesley, Reading, Mass, USA, 1994.

[79] L. J. Azevedo, J. E. Schirber, and E. M. Engler, "Se77 nuclear magnetic resonance in di-tetramethyltetraselenafulvalene phosphorous hexafluoride $[(TMTSF)_2PF_6]$ under pressure," *Physical Review B*, vol. 27, no. 9, pp. 5842–5845, 1983.

[80] N. Cao, T. Timusk, and K. Bechgaard, "Unconventional electrodynamic response of the quasi-one-dimensional organic conductor $(TMTSF)_2ClO_4$," *Journal de Physique I*, vol. 6, no. 12, pp. 1719–1726, 1996.

[81] H. K. Ng, T. Timusk, and K. Bechgaard, "Far-infrared properties of $(TMTSF)_2ClO_4$ at low temperatures," *Journal de Physique*, vol. 44, pp. C3-867–C3-872, 1983.

[82] K. Kornelsen, J. E. Eldridge, and G. S. Bates, "Far-infrared reflectivity of bis-tetramethyltetraselenafulvalene hexafluoroarsenate $[(TMTSF)_2AsF_6]$ through the spin-density-wave phase transition," *Physical Review B*, vol. 35, no. 17, pp. 9162–9167, 1987.

[83] P. M. Chaikin, P. Haen, E. M. Engler, and R. L. Greene, "Magnetoresistance and Hall effect in tetramethyl-tetraselenafulvalene-phosphorus hexafloride $[(TMTSF)_2PF_6]$," *Physical Review B*, vol. 24, no. 12, pp. 7155–7161, 1981.

[84] V. Vescoli, L. Degiorgi, B. Alavi, and G. Grüner, "The spin-density-wave gap in $(TMTSF)_2ClO_4$," *Physica B*, vol. 244, pp. 121–124, 1998.

[85] M. Dressel, L. Degiorgi, J. Brinckmann, A. Schwartz, and G. Grüner, "Optical response of the spin-density-wave ground state," *Physica B*, vol. 230-232, pp. 1008–1010, 1997.

[86] M. Dumm, A. Loidl, B. Alavi, K. P. Starkey, L. K. Montgomery, and M. Dressel, "Comprehensive ESR study of the antiferromagnetic ground states in the one-dimensional spin systems $(TMTSF)_2PF_6$, $(TMTSF)_2AsF_6$, and $(TMTTF)_2Br$," *Physical Review B*, vol. 62, no. 10, pp. 6512–6520, 2000.

[87] S. Watanabe, R. Kondo, S. Kagoshima, and R. Shimano, "Spin-density-wave gap in $(TMTSF)_2PF_6$ probed by reflection-type terahertz time-domain spectroscopy," *Physica Status Solidi (B)*, vol. 245, no. 12, pp. 2688–2691, 2008.

[88] S. Watanabe, R. Kondo, S. Kagoshima, and R. Shimano, "Observation of ultrafast photoinduced closing and recovery of the spin-density-wave gap in $(TMTSF)_2PF_6$," *Physical Review B*, vol. 80, no. 22, pp. 2204081-1–220408-4, 2009.

[89] S. Watanabe, R. Kondo, S. Kagoshima, and R. Shimano, "Ultrafast photo-induced insulator-to-metal transition in the spin density wave system of $(TMTSF)_2PF_6$," *Physica B*, vol. 405, no. 11, pp. S360–S362, 2010.

[90] H. H. S. Javadi, S. Sridhar, G. Grüner, L. Chiang, and F. Wudl, "Giant conductivity resonance in the spin-density-wave state of an organic conductor," *Physical Review Letters*, vol. 55, no. 11, pp. 1216–1219, 1985.

[91] S. Donovan, M. Dressel, L. Degiorgi, A. Schwartz, A. Virosztek, and G. Grüner, "Electrodynamic properties of $(TMTSF)_2PF_6$," *Synthetic Metals*, vol. 86, no. 1, pp. 2181–2182, 1997.

[92] A. Schwartz, S. Donovan, M. Dressel, L. Degiorgi, and G. Grüner, "Normal state electrodynamics of compounds with charge- and spin-density-wave ground states," *Physica B*, vol. 230–232, pp. 1005–1007, 1997.

[93] M. Dressel, "On the order parameter of Bechgaard salts," *Physica C*, vol. 317-318, pp. 89–97, 1999.

[94] K. Petukhov and M. Dressel, "Collective spin-density-wave response perpendicular to the chains of the quasi-one-dimensional conductor $(TMTSF)_2PF_6$," *Physical Review B*, vol. 71, no. 7, pp. 073101-1–073101-3, 2005.

[95] P. Zornoza, K. Petukhov, M. Dressel, N. Biskup, T. Vuletić, and S. Tomić, "Anisotropy and field-dependence of the spin-density-wave dynamics in the quasi one-dimensional conductor $(TMTSF)_2PF_6$," *European Physical Journal B*, vol. 46, no. 2, pp. 223–230, 2005.

[96] M. Dressel, K. Petukhov, and M. Scheffler, "Anisotropic SDW dynamics in $(TMTSF)_2PF_6$," *Journal of Low Temperature Physics*, vol. 142, no. 3-4, pp. 133–136, 2006.

[97] J. L. Musfeldt, M. Poirier, P. Batail, and C. Lenoir, "Microwave dielectric studies of the spin-density-wave state in $(TMTSF)_2PF_6$," *Physical Review B*, vol. 51, no. 13, pp. 8347–8356, 1995.

[98] J. L. Musfeldt, M. Poirier, P. Batail, and C. Lenoir, "*H-T* behavior of the spin density wave condensate in

$(TMTSF)_2AsF_6$," *Europhysics Letters*, vol. 30, no. 2, pp. 105–110, 1996.

[99] J. L. Musfeldt, M. Poirier, P. Batail, and C. Lenoir, "Magnetic-field behavior of the spin-density-wave state in $(TMTSF)_2AsF_6$," *Physical Review B*, vol. 52, no. 22, pp. 15983–15991, 1995.

[100] T. Vuletić, P. Auban-Senzier, C. Pasquier et al., "Coexistence of superconductivity and spin density wave orderings in the organic superconductor $(TMTSF)_2PF_6$," *European Physical Journal B*, vol. 25, no. 3, pp. 319–331, 2002.

[101] N. Kang, B. Salameh, P. Auban-Senzier, D. Jérome, C. R. Pasquier, and S. Brazovskii, "Domain walls at the spin-density-wave endpoint of the organic superconductor $(TMTSF)_2PF_6$ under pressure," *Physical Review B*, vol. 81, no. 10, pp. 100509-1–100509-4, 2010.

[102] R. Bozio, C. Pecile, K. Bechgaard, F. Wudl, and D. Nalewajek, "Infrared study on the formation of charge density waves in $(TMTSF)_2X$ ($X = ReO_4^-$ and PF_6^- at atmospheric pressure," *Solid State Communications*, vol. 41, no. 12, pp. 905–910, 1982.

[103] K. Kikuchi, I. Ikemoto, K. Yakushi, H. Kuroda, and K. Kobayashi, "Temperature dependence of the reflectance spectrum of $(TMTSF)_2ClO_4$," *Solid State Communications*, vol. 42, no. 6, pp. 433–435, 1982.

[104] H. K. Ng, T. Timusk, J. M. Delrieu, D. Jérome, K. Bechgaard, and J. M. Fabre, "Observation of a gap in the farinfrared magneto-absorption of $(TMTSF)_2ClO_4$: possibility of one-dimensional fluctuating superconductivity," *Journal de Physique Lettres*, vol. 43, pp. 513–519, 1982.

[105] T. Timusk, "Quasi one-dimensinoal conductors: the far infrared problem," in *Low-Dimensional Conductors and Superconductors*, D. Jérome and L. G. Caron, Eds., vol. 155 of *NATO ASI B Series, Physics*, pp. 275–2284, Plenum Press, London, UK, 1987.

[106] T. Timusk, "Infrared properties of exotic superconductors," *Physica C*, vol. 317-318, pp. 18–29, 1999.

[107] H. Schwenk, K. Andres, and F. Wudl, "Resistivity of the organic superconductor ditetramethyltetraselenafulvalenium perchlorate, $(TMTSF)_2ClO_4$, in its relaxed, quenched, and intermediate state," *Physical Review B*, vol. 29, no. 1, pp. 500–502, 1984.

[108] D. Pedron, R. Bozio, M. Meneghetti, and C. Pecile, "Electronic interactions in the organic conductors $(TMTSF)_2X$ ($X = CIO_4$ and PF_6) and $(TMTTF)_2X$ ($X =$ Br and PF_6) from their infrared spectra," *Physical Review B*, vol. 49, no. 16, pp. 10893–10907, 1994.

[109] W. A. Challener, P. L. Richards, and R. L. Greene, "Far infrared properties of $(TMTSF)_2ClO_4$," *Journal de Physique*, vol. 44, pp. C3-873–C3-878, 1983.

[110] W. A. Challener, P. L. Richards, and R. L. Greene, "Far infrared measurements of $(TMTSF)_2ClO_4$," *Solid State Communications*, vol. 51, no. 10, pp. 765–768, 1984.

[111] J. E. Eldridge, C. C. Homes, F. E. Bates, and G. S. Bates, "Far-infrared powder absorption measurements of some tetramethyltetraselenafulvalene salts $[(TMTSF)_2X]$," *Physical Review B*, vol. 32, no. 8, pp. 5156–5162, 1985.

[112] C. C. Homes and J. E. Eldridge, "Lattice-mode coupling to the charge-density wave in $(TMTSF)_2ReO_4$ (where TMTSF is bis-tetramethyltetraselenafulvalene)," *Physical Review B*, vol. 40, no. 9, pp. 6138–6143, 1989.

[113] C. C. Homes and J. E. Eldridge, "Infrared optical properties of $(TMTSF)_2ReO_4$ and $(TMTSF)_2BF_4$ (where TMTSF is tetramethyltetraselenafulvalene) compared with several model calculations," *Physical Review B*, vol. 42, no. 15, pp. 9522–9533, 1990.

[114] J. E. Eldridge and C. C. Homes, "Vibrational assignments in the conductivity spectra of semiconducting $(TMTSF)_2ReO_4$ and $(TMTSF)_2BF_4$ (where TMTSF is tetramethyltetraselenafulvalene) for radiation polarized perpendicular to the chains," *Physical Review B*, vol. 43, no. 17, pp. 13971–13977, 1991.

[115] M. Dressel, M. Dumm, T. Knoblauch, and M. Masino, "Comprehensive optical investigations of charge order in organic chain compounds $(TMTTF)_2X$," *Crystals*, vol. 2, pp. 528–578, 2012.

[116] M. Krauzman, H. Poulet, and R. M. Pick, "Resonant Raman scattering in a bis-tetramethyltetraselenafulvalene- hexafluorophosphate $[(TMTSF)_2PF_6]$ single crystal," *Physical Review B*, vol. 33, no. 1, pp. 99–105, 1986.

[117] G. Rindorf, H. Soling, and N. Throup, "Di(4, 4′, 5, 5′-tetramethyl-2, 2′-bi-1,3-diselenolyliden)ium perrhenate, $C_{20}H_{24}Se_8^+ .ReO_4^-$, $(TMTSF)_2ReO_4$. Detailed superstructure at 120 K," *Acta Crystallographica C*, vol. 40, pp. 1137–11139, 1984.

[118] T. J. B. M. Janssen, A. S. Perel, A. M. Gerrits et al., "Far-infrared spectroscopy of the field-induced spin-density-wave gap in $(TMTSF)_2ClO_4$," *Physical Review B*, vol. 46, no. 13, pp. 8663–8666, 1992.

[119] A. S. Perel, J. S. Brooks, C. J. G. N. Langerak et al., "Magnetic-field-dependent energy levels in a highly anisotropic electronic material," *Physical Review Letters*, vol. 67, no. 15, pp. 2072–2075, 1991.

[120] R. Ellison, M. Reedyk, and K. Behnia, "Far-infrared electrodynamic response of $(TMTSF)_2ClO_4$ in the normal and superconducting states," *Physical Review B*, vol. 66, no. 1, pp. 125081–125084, 2002.

[121] B. Gorshunov, S. Kaiser, and M. Dressel, "THz opticalproperties of $(TMTSF)_2ClO_4$ and $(TMTSF)_2PF_6$," in press.